

### **Central Lancashire Online Knowledge (CLoK)**

Title	On the Performance Analysis of UE-VBS-Based Wireless Communications:		
	Network Outages, Resource Utilization, and Optimization		
Type	Article		
URL	https://clok.uclan.ac.uk/id/eprint/55934/		
DOI	https://doi.org/10.1109/ACCESS.2025.3573846		
Date	2025		
Citation	Ioannou, Iacovos I., Khalifeh, Ala', Nagaradjane, Prabagarane,		
	Christophorou, Christophoros, Vassiliou, Vasos, Neokleous, Orestis and		
	Pitsillides, Andreas (2025) On the Performance Analysis of UE-VBS-Based		
	Wireless Communications: Network Outages, Resource Utilization, and		
	Optimization. IEEE Access, 13. pp. 94585-94610. ISSN 2169-3536		
Creators	Ioannou, Iacovos I., Khalifeh, Ala', Nagaradjane, Prabagarane,		
	Christophorou, Christophoros, Vassiliou, Vasos, Neokleous, Orestis and		
	Pitsillides, Andreas		

It is advisable to refer to the publisher's version if you intend to cite from the work. https://doi.org/10.1109/ACCESS.2025.3573846

For information about Research at UCLan please go to <a href="http://www.uclan.ac.uk/research/">http://www.uclan.ac.uk/research/</a>

All outputs in CLoK are protected by Intellectual Property Rights law, including Copyright law. Copyright, IPR and Moral Rights for the works on this site are retained by the individual authors and/or other copyright owners. Terms and conditions for use of this material are defined in the http://clok.uclan.ac.uk/policies/



Received 8 May 2025, accepted 22 May 2025, date of publication 28 May 2025, date of current version 4 June 2025.

Digital Object Identifier 10.1109/ACCESS.2025.3573846



# On the Performance Analysis of UE-VBS-Based Wireless Communications: Network Outages, Resource Utilization, and Optimization

IACOVOS I. IOANNOU<sup>®1,2</sup>, (Senior Member, IEEE), ALA' KHALIFEH<sup>®3</sup>, PRABAGARANE NAGARADJANE<sup>4</sup>, CHRISTOPHOROS CHRISTOPHOROU<sup>2,5</sup>, VASOS VASSILIOU<sup>1,2</sup>, (Senior Member, IEEE), ORESTIS NEOKLEOUS<sup>1,2</sup>, AND ANDREAS PITSILLIDES<sup>®1,6</sup>

Corresponding author: Iacovos I. Ioannou (ioannou.iakovos@ucy.ac.cy)

This work was supported in part by European Union's Horizon 2020 Research and Innovation Program under Grant 739578; in part by the Distributed Artificial Intelligence-Driven Open and Programmable Architecture for 6G Networks (ADROIT6G) Project of the Smart Networks and Services Joint Undertaking (SNS JU) project under Grant 101095363; and in part by the Government of Cyprus through the Deputy Ministry of Research, Innovation and Digital Policy.

**ABSTRACT** User Equipment as a Virtual Base Station (UE-VBS) computing paradigm represents a significant advancement in wireless networking. It enables User Equipment (UE) to form: i) Virtual Base Stations (VBSs) by dynamically integrating Cluster Heads (referred to as UE-VBS<sub>CH</sub>), or Virtual Relays (referred to as UE-VBS<sub>RI.</sub>), in the far-edge domain. This research focuses on enhancing the Quality of Service (QoS) (and thereby improving user experience) in networks supported by UE-VBS computing through outage prediction, network optimization, and advanced wireless techniques. In addition, the paper presents a detailed outage probability analysis and explores the trade-off between efficiency and reliability (namely, spectral and energy efficiency and link-level reliability (outage probability)), which are core contributions of this work. For a representative urban density of 2 UEs per m<sup>2</sup>, a single-hop UE-VBS slice lowers the outage probability from 0.78 to 0.23, raises the peak area-spectral efficiency to 4.3 bit s<sup>-1</sup>  $Hz^{-1}$ ( $\approx 4.8 \times$  the baseline), and delivers an energy efficiency of  $2.4 \times 10^5$  bit J<sup>-1</sup> ( $\approx 4.6 \times$  improvement). These concrete figures substantiate the claimed gains and illustrate how UE-VBS computing simultaneously improves efficiency and reliability. Specifically, it provides a thorough examination of UE-VBS computing's capacity to enhance service quality, reduce congestion, and promote energy efficiency. Also, it empirically confirms UE-VBS computing's superior performance, including mitigating coverage gaps coverage gaps are localized areas inside a nominally covered cell where received SINR falls below the outage threshold because of shadowing or cell-edge distance), optimizing network traffic, and reducing battery consumption compared to traditional networks/non-UE-VBS computing-supported networks. Enhanced QoS aims to minimize the challenges associated with restricted network coverage, ensuring consistent data transmission rates and improving overall user satisfaction. The potential exists for adopting effective network traffic offloading to mitigate the heavy traffic on primary base stations known as Next Generation Node B (gNodeB). Consequently, this can result in enhanced spectrum utilization and heightened data throughput. Leveraging UE-VBS computing also contributes to power conservation and fosters sustainability.

**INDEX TERMS** UE-VBS, network system outage, resource analysis, optimization.

The associate editor coordinating the review of this manuscript and approving it for publication was Miguel López-Benítez.

<sup>&</sup>lt;sup>1</sup>Department of Computer Science, University of Cyprus, 1678 Nicosia, Cyprus

<sup>&</sup>lt;sup>2</sup>CYENS—Center of Excellence, 1678 Nicosia, Cyprus

<sup>&</sup>lt;sup>3</sup>Department of Computer Science, German Jordanian University, Amman 11180, Jordan

<sup>&</sup>lt;sup>4</sup>Department of ECE, Sri Sivasubramaniya Nadar College of Engineering, Chennai 603110, India

<sup>&</sup>lt;sup>5</sup>Department of Computer Science, University of Central Lancashire (UCLan), 7080 Larnaca, Cyprus

<sup>&</sup>lt;sup>6</sup>Department of Electrical and Electronic Engineering, University of Johannesburg, Johannesburg 2006, South Africa



#### I. INTRODUCTION

Our investigation is centered on demonstrating the superior performance of the User Equipment as a Virtual Base Station (UE-VBS)-assisted networks (introduced in [1], [2], [3]) compared to traditional cellular networks. User Equipment as a Virtual Base Station (UE-VBS) is the paradigm in which ordinary user devices are promoted, under software control, into ad-hoc small-cell elements that support the macro network. Based on instantaneous channel quality, residual battery, and geometric position, a device may function either as a virtual base-station cluster head-aggregating and forwarding traffic for nearby users—or as a virtual relay that extends coverage toward the cell edge. Crucially, radioresource management and security remain under gNodeB control, so the air-interface standard itself is not altered. The concept was first introduced and experimentally explored in [1], [2], and [3], where UE-VBS nodes were shown to offload macro-cell traffic, heal coverage gaps, and improve both spectral and energy efficiency, especially in dense urban deployments. We aim to show that UE-VBS computing offers a compelling solution by addressing key challenges such as mitigating coverage gaps (i.e., localized zones inside a nominally covered cell where the received SINR falls below the outage threshold because of heavy shadowing or large path loss) enhancing network traffic management, and reducing power consumption. By elevating suitably positioned UEs to virtual cluster heads or relays, the system forms short D2D hops that bypass the deep-fade segment and re-establish a high-SINR route to the gNodeB, thereby closing the coverage gap. To align our contributions with the demonstrated benefits of the UE-VBS-based network, the following sections explicitly connect the analytical and simulation results with the advantages provided by this paradigm.

The benefits of UE-VBS computing are manifold, including:

- It enhances the Quality of Service (QoS) by reducing coverage gaps within the cell, ensuring consistent data rates, and improving the overall user experience.
- It efficiently offloads network traffic by integrating UE-VBS-enabled devices, reducing the load on the main base station (Next Generation Node B or gNodeB) [4] and optimizing spectrum efficiency and data throughput through intelligent bandwidth allocation.
- It conserves power by reducing radio wave propagation distance and intelligently sharing power with UE-VBS clients, contributing to environmental sustainability and incentivizing client participation.

In the analytical part of this study, we employ the Free Space Path Loss (FSPL) model to simulate the ideal conditions under which signal strength decays as a function of distance in a free-space environment, with no obstacles affecting the transmission. Additionally, we incorporate Additive White Gaussian Noise (AWGN) to account for random fluctuations in the signal, ensuring a more comprehensive representation of noise-induced degradation in

the communication channel. These assumptions help create a simplified yet effective framework for evaluating the system's performance, providing baseline results that serve as a comparison to more complex models used in the simulation. In addition to the FSPL model used for the analytical results, this study employs the LOGD path loss model in the numerical simulations to account for more realistic environmental effects on signal propagation. The LOGD model provides a more practical representation of wireless signal behavior in urban environments, where obstacles such as buildings and other structures cause significant attenuation. By incorporating the LOGD model, we can simulate the variations in signal strength due to factors like shadowing and path loss exponent, making the analysis more applicable to real-world network deployments. This approach allows us to contrast the idealized analytical results with more complex, real-world scenarios.

The novelty of this paper lies in its comprehensive and in-depth analysis of UE-VBS computing, focusing on its outage probability, resource allocation improvements, and overall performance enhancement in wireless networks. This study provides new insights into the trade-offs between system efficiency and reliability by utilizing analytical models (such as FSPL with AWGN) and more realistic simulations (using the LOGD path loss model). Additionally, the paper introduces a novel method for evaluating spectral and energy efficiency in multi-hop UE-VBS-supported networks, which has not been thoroughly explored in existing literature. This multi-dimensional evaluation framework offers a clearer understanding of how the UE-VBS computing paradigm can optimize network traffic, reduce outages, and enhance spectrum utilization, particularly in high-density urban environments.

To better connect our contributions with these benefits, the remainder of the paper is structured to first analytically demonstrate these advantages and then validate them through network simulations. Specifically, our focus centers on addressing the challenge of improving QoS, particularly the outage probability and the network efficiency, within the context of UE-VBS computing (see section II-A1).

More specifically, this paper aims to demonstrate that UE-VBS-assisted networks outperform traditional cellular networks in terms of performance. The system offers several key benefits. First, it increases Quality of Service (QoS) by reducing potential coverage gaps within the cell area, resulting in fewer inconsistencies in data rates and enhancing the overall user experience. Second, it offloads network traffic by reducing the number of independent channels connected to the gNodeB simultaneously, as some data processing is allocated to UE-VBS-enabled devices. The UE-VBS improves spectrum efficiency, measured in bits/s/Hz, by allocating bandwidth based on the throughput of new network paths created. By leveraging off-band frequencies and geographical knowledge, these connections to the gNodeB can lead to a higher overall data rate. Specific backhaul bandwidth for UE-VBS devices could



also be reserved, depending on network design. Finally, the system contributes to power saving by shortening the radio wave transmission distance from the gNodeB to devices, reducing signal loss, and allowing for lower transmission power. By effectively sharing power with UE-VBS clients, who may be incentivized through free data, discounts, or additional gadgets, the overall power consumption of the cellular network can be significantly reduced. In what follows, we demonstrate the above-mentioned central benefits analytically and provide a network simulation. This analytical and simulation-based demonstration directly supports our contributions by quantifying the improvements in QoS, outage probability, and network efficiency. This work addresses the problem of QoS improvement and, more specifically, the outage probability and network efficiencies.

Overall, this study presents a novel analysis of UE-VBS computing, focusing on its outage likelihood, resource allocation enhancements, and performance improvements in congested circumstances. The novelty of this research lies in its pioneering approach to wireless networking, epitomized by the introduction of the UE-VBS computing paradigm. UE-VBS computing harnesses the inclusion of UE-VBS with dynamic cluster heads and relays drawn from a pool of selected or volunteer clients. This novel approach represents a paradigm shift in optimizing network resources and enhancing network performance, particularly in congested scenarios. The research highlights the transformative nature of UE-VBS computing by substantiating its superiority over traditional cellular networks, offering quantifiable benefits such as elevated QoS, diminished coverage gaps, reduced gNodeB load through intelligent network traffic offloading, and minimized power consumption via judicious signal propagation control.

This study's contribution is unique in its holistic exploration, blending analytical rigour and network simulations, with a central focus on enhancing QoS, reducing outage probabilities, and optimizing network efficiency within the innovative UE-VBS framework. Note that, to the best of our knowledge and after conducting extensive research, a similar examination of UE-VBS does not exist in the literature. The contributions of the paper can be summarized as follows:

- Provides a comprehensive analysis of UE-VBS fundamental concepts and advantages.
- Demonstrates UE-VBS computing potential to improve the quality of service, mitigate congestion, and conserve energy.
- Highlights notable performance advantages over conventional (i.e., non-UE-VBS-assisted) cellular networks.
- Addresses coverage gaps, network traffic, and battery consumption challenges.
- Efficient network traffic offloading: UE-VBS allows user devices to handle some network traffic, reducing the burden on the main base station (eNodeB). The UE-VBS distributes the load more evenly, preventing congestion and improving overall network efficiency.

- optimized spectrum utilization and data throughput: UE-VBS intelligently allocates bandwidth to connected devices based on current network conditions. The UE-VBS ensures that the available spectrum is used more efficiently, allowing more data to be transmitted faster, particularly in areas with high user density.
- Power conservation: By using nearby devices as relays, UE-VBS reduces the distance that signals need to travel. The UE-VBS minimizes the power required for transmission, leading to lower energy consumption and extended battery life for user devices.
- Provides both analytical analysis and network simulations to substantiate advantages.
- Primary focuses on improving QoS, outage likelihood, and network efficiency in UE-VBS-assisted networks.

The rest of the paper is structured as follows: Section II offers a comprehensive overview of the fundamental concepts and existing scholarly works about UE-VBS. Section III delineates the key assumptions employed in the analysis of the UE-VBS system. Next, Section IV is focused on developing a model for the UE-VBS system. Section V explores the analytical components regarding the UE-VBS. Moreover, Section VI introduces a numerical simulation model that enables an investigation of the precision of the preceding analytical model. Section VII demonstrates the findings, encompassing numerical results compared to analytical solutions. Finally, Section VIII summarizes significant findings, evaluates the analysis and simulation's effectiveness, recognises underlying assumptions, and delineates potential avenues for further research.

The notations used in the rest of the research paper are also given in Table 1.

### II. BACKGROUND INFORMATION AND LITERATURE REVIEW

This section provides the background information and a literature review regarding UE-VBS.

#### A. BACKGROUND INFORMATION

This subsection provides the background information regarding our approach and the UE-VBS concept, which is explained briefly below.

#### 1) THE UE-VBS COMPUTING

The UE-VBS computing (introduced in [1], [2], [3]): In our concept, the fundamental assumption of our model is that selected or volunteering clients (to become UE-VBS) of the network will have specialized software (a mobile native app) installed on their devices that, when needed, would allow them to become a Cluster Head (as UE-VBS<sub>CH</sub>) or a Relay (as UE-VBS<sub>RL</sub>) depending on the requirements, as depicted in Fig. 1. These ad hoc networks are formed by a graph/network architecture that employs an algorithm that optimizes the network resources. The algorithm is discussed briefly in the paper, as most of the content deals with the modeling of the networks and how the modeling



TARIF 1	Main mathematical	notations used	in this research

Symbol	Description	Calculated in Eq.	Used in Eq.
U	Set of UEs in a cell	-	1, 2
$R_{\min}$	Minimum data rate acceptable by UEs in $U$	6	14, 15, 16, 26
$U_{UE-VBS}$	Subset of U with UE-VBS capabilities (app installed)	-	3, 5, 7
$U_{UE-VBS}_{\mathrm{CH}}$	Subset of $U_{UE}$ — $V_{BS}$ , which are the UE- VBS-enabled devices chosen to be cluster heads	-	11, 12, 14
$U_{UE-VBS_{ m RL}}$	Subset of $U_{UE}$ — $VBS$ , which are the UE- VBS-enabled devices chosen to be relay devices	-	13, 15, 16
$S_{ij}$	UE-VBS clusters between devices	-	18, 24
Φ	Set describing the randomly generated cluster process	-	23, 24
C.	The clusters include individual points of the cluster	-	22, 23
l(r)	Power loss function for a channel at a distance r	5	25
f(x)	Probability Density Function (PDF) of a random variable x	-	3, 6, 14
F(x)	Cumulative Distribution Function (CDF) of random variable x	-	3, 6
$h_X$	Channel x's multiplicative fading noise	-	5, 12, 14
$G_X$	Channel x's channel gain	5	12
$P_X$	Channel x's transmitting power	5	15
W	Additive White Gaussian Noise (AWGN)	5	12, 22
$I_X$	Channel x's interfering power	12	22
λ	Intensity of Poisson point process (PPP)	1, 2	24, 26
$\lambda_c$	Intensity of points (UEs) within a cluster	2	24, 26
SINR	Signal-to-Interference-plus-Noise Ratio	6	7, 12, 13, 26
SINR <sub>TH</sub>	Threshold for SINR, below which an out- age occurs	6	17, 22, 23, 26
SNR	Signal-to-Noise Ratio	17	22
SNR <sub>TH</sub>	Threshold for SNR, below which an outage occurs	17	-
Pout	Outage probability	17	7, 23, 24, 26
$P_t$	Transmitting power at any point in the net- work	15	16
$P_{tot}$	Total power consumed in the system	15	16
$B_{UE-VBS}$	Bandwidth allocated to a UE-VBS connec- tion	6	13, 26
$B_{SYS}$	Total system bandwidth	10	13
$\eta_{\rm sysSE}$	System spectral efficiency	13	11, 26
$\eta_{sysEE}$	System energy efficiency	14	26
R	Data rate in the system	9	14, 26
r	Distance between transmitter and receiver	5	22
σ	Standard deviation in Thomas cluster pro- cess	2	23, 24
a	Path loss exponent	22	25
γ	Dynamic power loss factor depending on data rate	15	16
β	Average power loss factor accounting for antenna gain	15	16
$N_{0}$	Noise spectral density	-	12, 5

could improve the performance measured by the network's spectral and energy efficiency, which is defined later in the paper. All devices are planned to act on the UE-VBS layer, a new layer placed right above the physical layer (bottom of Layer 2 in the Evolved Universal Terrestrial Radio Access Network (e-UTRAN) protocol stack [4]). Moreover, most of the contributions available in the open literature have made some advancements in introducing autonomous agents [5] in UE-VBS-enabled devices and network formation [3]. Nevertheless, outage analysis in the context of UE-VBS-assisted networks has not been addressed. The system considered in our work is shown in Fig. 1. The UE-VBS computing has two major elements: the UE-VBS<sub>CH</sub> and the UE-VBS<sub>RL</sub>, as explained below:

 UE-VBS<sub>CH</sub>: These devices will provide relay access to the main base station (eNodeB) either directly or through UE-VBS<sub>RL</sub> devices and to the UE-clients that are chosen to be included in the cluster. Inside the cluster, UE clients

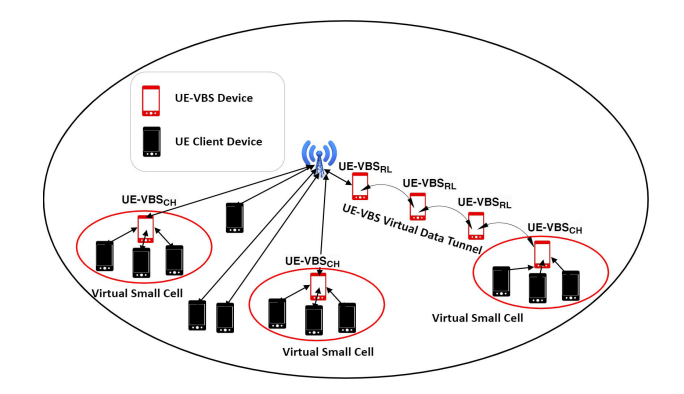


**FIGURE 1.** A graphical depiction of UE-VBS computing paradigm showing Virtual Base Stations acting as Small Cells, with UE-VBS<sub>CH</sub> and UE-VBS<sub>RL</sub> nodes [1].

connect to the UE-VBS $_{CH}$  using an in-band or out-band (cellular/mmWave for 5G or WiFi ) OFDM signal to avoid interference.

UE-VBS<sub>RL</sub>: These devices will be used to reach a
 UE-VBS<sub>CH</sub> or a single UE-client that would be in a
 location inside the cell that has bad or medium Channel
 Quality Index (CQI) reception of the signal from
 gNodeB, which is below a satisfactory level, and would
 provide a sufficient Device-to-Device (D2D) signal to
 deliver seamless uplink and downlink connection to the
 network.

#### 2) POISSON CLUSTERING PROCESSES

A constant assumption that we make throughout this work is that UE-device locations in an urban environment can be probabilistically described as Poisson Cluster Processes (PCP). This assumption is valid because it has been proved to be a good approximation in many recent works for an arbitrary distribution of devices in urban environments [6], [7]. To be more exact, we use a  $Cox^1$  process called the Thomas cluster process [8]. This specific process can be described as follows. Firstly, Poisson-distributed points are uniformly distributed in a 2D area. A brief description of the PCP is that given a density/intensity  $\lambda$  of clusters in an area A, we can say that the number of devices in our area/region will be a Poisson Random Variable (RV) with overall intensity of  $\lambda A$ . As our area is in 2D, the X and Y axes of the given Poisson RV locations are uniformly distributed in area A with width equal to W and length equal to L, resulting in A being W \* L. Thus, we can say that the probability of having n a number of

<sup>&</sup>lt;sup>1</sup>A Cox process, also known as a doubly stochastic Poisson process, is a point process where the intensity measure is random. This characteristic differentiates it from a standard Poisson process, where the intensity measure is fixed and known. In a Cox process, the intensity measure is modeled by a random measure, leading to a hierarchical or two-stage model: first, a realization of the random measure is generated, and then, conditioned on this realization, points are scattered according to a Poisson process with the given random intensity.



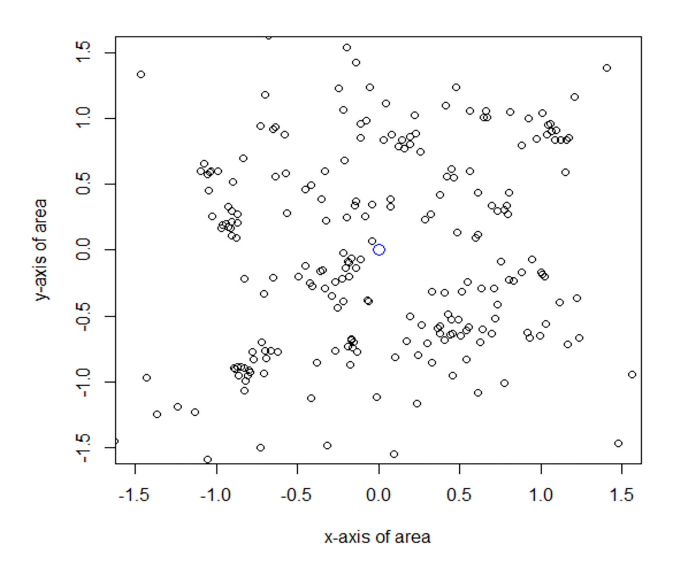


**FIGURE 2.** The generated clusters with the use of the Thomas clustering process.

devices in A is given below.

$$Pr\{N(A) = n\} = \frac{(\lambda A)^n}{n!} e^{-\lambda A} \tag{1}$$

Then, the cluster points themselves  $Y = \{y_1, y_2, ..., y_k\}$  are distributed in an isotropic Gaussian manner around the central positions x (set of all cluster centers of length k) of the cluster, whose Probability Density Function (PDF) is given by the following equation:

$$f_Y(y) = \frac{1}{2\pi\sigma^2} \exp\left(-\frac{||y||^2}{2\sigma^2}\right) \tag{2}$$

where  $\sigma$  is the standard deviation (spread) and ||y|| is the Euclidean distance of the cluster point from the center of the cluster. The number of devices in each cluster is again a Poisson RV with an intensity of  $\lambda_c$ . The combination of these processes produces Thomas clustering. A generated example is illustrated in Fig. 2.

#### 3) POISSON POINT PROCESS INTENSITY

The Poisson Point Process Intensity (PPPI), denoted by  $\lambda$ , is a fundamental concept in stochastic geometry and spatial statistics. It represents the average rate or density of events or points in a given spatial region (in our case, the UEs). It is defined as the expected number of points or events per unit area or volume within that region. Mathematically,  $\lambda$  can take non-negative real values, i.e.,  $\lambda \geq 0$ , and it characterises the random distribution of points in space. A higher  $\lambda$  implies a higher point density, while a lower  $\lambda$  indicates a lower point density. The Poisson Point Process (PPP) is often used to model random events such as the occurrence of disease cases in a geographic area, the distribution of trees in a forest, or the locations of customers in a retail store, where the intensity parameter  $\lambda$  plays a crucial role in determining the overall spatial pattern and clustering of these events.

Let  $\lambda$  be the intensity of UEs per unit area (UEs/m<sup>2</sup>) in a particular region. If you have a total of N UEs in that region, and the area of the region is A (in square meters), then you can calculate the intensity ( $\lambda$ ) as  $\lambda = \frac{N}{A}$ , where  $\lambda$  represents the density of UEs in the area A.

#### 4) OUTAGE PROBABILITY

Outage probability, denoted by  $P_{\text{out}}$ , is a fundamental concept in telecommunications and wireless communication systems, representing the likelihood that a communication link or channel experiences an interruption or failure, typically due to fading, interference, or other impairments. It is a critical performance metric, especially when reliable communication is essential. Outage probability can be mathematically formulated as  $P_{\text{out}} = P(\text{SNR} < \text{SNR}_{\text{TH}})$ , where SNR represents the Signal-to-Noise Ratio, and SNR<sub>TH</sub> is the threshold SNR below which the communication link is considered to be in an outage. Outage probability varies with different communication systems and environments; for example, in wireless networks, it can be influenced by path loss, fading models, and interference levels. The values of outage probability typically range from 0 to 1, with lower values indicating a more reliable communication link and higher values indicating a less reliable or "outage" link. In practice, outage probability is a critical parameter used to design and optimize communication systems for desired reliability levels. It is often used to evaluate the effectiveness of various communication strategies and algorithms in adverse conditions.

#### B. LITERATURE REVIEW RELEVANT TO UE-VBS

Deploying UE-VBSs plays a crucial role in contemporary communication networks, significantly improving network performance and efficiency [2], [3], [9], [10], [11], [12], [13], [14], [15]. Their primary objective is to enhance data rates, coverage, and overall network capacity. The literature review spans many methodologies, including Affinity Propagation Clustering (APC), Machine Learning-based strategies, and novel algorithms such as Modified Affinity Propagation Clustering (MAPC) and Multi-Hop Load Balanced Geographical Path selection (MLGP). In addition, this study delves into the examination of Wireless Network Virtualization (WNV) as a means to enhance resource allocation and optimize the Virtual Base Station association. Furthermore, the paper examines research efforts to mitigate power consumption in heterogeneous 5G networks and improve energy efficiency in small cell deployments inside ultra-dense network environments. In conclusion, this thorough analysis provides insight into the dynamic nature of network optimization within contemporary communication systems.

One method for choosing UE-VBSs entails the utilization of APC, as suggested by the authors in the referenced publication [9]. This methodology aims to determine the optimal selection of UE-VBSs that can effectively enhance network performance by complementing the current Small



Cell Base Stations (SCBSs). The simulation's findings demonstrate this methodology's advantages and constraints, specifically concerning its potential scalability. Affinity Propagation Clustering (APC) merits special attention because it (i) requires no a-priori choice of cluster count, (ii) converges to a globally optimal set of exemplars, and (iii) copes well with the irregular UE topologies typical of dense urban cells [9], [16]. These properties make APC attractive for small-to-medium-scale deployments where accurate cluster-head placement directly boosts spectral and energy efficiency. The principal drawback is scalability: the similarity matrix and message-passing updates grow as  $\mathcal{O}(N^2)$ , so memory and run-time become prohibitive once the candidate pool exceeds a few thousand UEs [10]. Recent studies, therefore, combine APC's accuracy with downselection heuristics, or replace it with lighter schemes such as MAPC, IMCA, or ML-assisted classifiers when ultra-dense scenarios are targeted.

The authors of [2] investigate a methodology based on machine learning to choose and activate UE-VBSs dynamically and effectively. Using unsupervised techniques for clustering user equipment and subsequent classification using supervised learning, the identification of as many suitable UEs as possible as UE-VBSs is achieved. The study provides evidence of the efficacy of Decision Trees in appropriately classifying these User Entities. In particular, the trained Decision Tree applies a sequence of threshold tests—residual battery  $b_{\rm res} \geq 0.70$ , uplink SINR SINR  $\geq 15$  dB, distance to gNodeB  $d \leq 300$  m, CPU speed  $f_{\rm CPU} \geq 1.4$  GHz, and RAM  $R \geq 2$  GB—to nominate each UE as a VBS candidate, guaranteeing both link reliability and sufficient on-device resources.

To improve the efficiency of network operations and backhauling optimization, the authors of [3] propose the utilization of two algorithms: The MAPC and the Multi-Hop Load Balanced Geographical Path selection algorithms. These strategies aim to strategically choose UE-VBSs to enhance network performance by increasing capacity and data rates in locations with limited infrastructure. Specifically, MAPC selects cluster-head UEs by minimizing a composite cost function that jointly accounts for residual device energy (to reduce power consumption), average intra-cluster distance (to limit latency and path loss), and achieved spectral efficiency over the D2D links, thereby balancing energy use, delay, and throughput.

The authors of [10] suggest a two-stage machine-learning methodology for the dynamic selection and activation of the UE-VBS. Clustering techniques such as K-Means and MeanShift are utilized to group Users' Equipment, followed by the application of supervised Machine Learning classification algorithms to ascertain the eligibility of the UEs. The methodology above attains a notable level of precision, particularly when employing the Random Forest classifier.

The Initializing Matching Connection algorithm (IMCA) is proposed in [11] to dynamically select Virtual Small Base Stations in ultra-dense 5G networks. The IMCA protocol

emphasizes the establishment of the primary link between client User Equipment and eligible UEs, which leads to the creation of clusters and the activation of UE-VBSs to mitigate network congestion.

The article [12] discusses the utilization of Wireless Network Virtualization to tackle the resource allocation and VBS association problem in cellular Device-to-Device communication networks. This study introduces a heuristic method to address the tasks of mode selection, UE and VBS matching, and resource allocation. The study aims to demonstrate the efficacy of the suggested approach.

The article referenced as [13] presents the Grid Assisted Affinity Propagation Clustering (GAPC) method as a means to improve spectral efficiency within the context of Cell-based Virtual Small Cell (CHVSC) services. This approach integrates clustering and member selection methodologies to enhance overall performance.

The study conducted by the authors in reference [14] centers on the objective of reducing power consumption in heterogeneous 5G networks by optimizing User Equipment association, backhauling, and sleep control mechanisms of small base stations. The system utilises intelligent backhauling algorithms and load-sharing techniques to maximise the network's energy efficiency.

The authors' study, as described in reference [15], proposes a deployment approach that seeks to enhance energy efficiency in small cells inside ultra-dense networks. The authors suggest using the Efficient Cell modeling (ECM) method and the Binary Particle Swarm optimization-based Small Cell Deployment (BPSD) strategy as strategies to enhance energy efficiency and connectivity.

Overall, the existing approaches in the field of UE-VBS include APC, MAPC, Machine Learning techniques, IMCA, GAPC, and MLGP. These researches collectively improve the performance of networks in terms of data speeds, coverage, capacity, and energy efficiency. The authors give the selection of User Equipment and Virtual Base Station considerable importance as a means to address challenges associated with scalability, network congestion, and power consumption in evolving communication systems. This statement underscores the ongoing endeavours being undertaken to enhance network operations in light of evolving requirements. However, the current body of literature needs more investigation to analyze physical channel characteristics related to UE-VBS deployment and the likelihood of encountering service disruptions when utilizing this technology. This investigation focuses on the aforementioned challenges.

#### 1) POSITIONING AND NOVELTY OF THE PRESENT WORK

Previous UE-VBS papers each tackled only a single slice of the problem space: APC head-selection shapes clusters but stops short of system-level performance [9]; ML-based nomination refines head choice yet ignores multi-hop propagation and energy cost [2]; two-stage ML frameworks (K-Means/Mean-Shift + Random Forest) improve selection accuracy but still neglect end-to-end



**TABLE 2.** Qualitative advantage of the proposed analysis over prior UE-VBS literature.

Reference	Main focus / limitation	Joint Outage + SE/EE
Swain <i>et al</i> . [9]	APC cluster-head placement; no outage or efficiency analysis	Х
Ioannou <i>et al</i> . [2]	ML head nomination; per-UE metrics only	X
Veluswami <i>et al</i> . [10]	Two-stage ML selector; ignores link reliability	X
Venkateswararao et al. [3]	MAPC/MLGP back-haul optimisation; deterministic geometry	×
Venkateswararao et al. [11]	IMCA link matching; fixed topology	×
Danisya <i>et al.</i> [13]	GAPC maximises SE; ignores outage/EE	×
Wang <i>et al</i> . [12]	WNV VBS association; no relays considered	X
Venkateswararao et al. [14]	Sleep-mode power saving; omits SE and outage	X
Venkateswararao et al. [15]	ECM+BPSD small-cell placement; no end-to-end QoS	X
This paper	Closed-form outage plus spectral- efficiency (SE) and energy- efficiency (EE) evaluation for networks modelled by a Poisson- cluster process (PCP) and a log-distance (LOGD) path-loss law; includes hop/density trade-off with concrete 4.8× (SE) / 4.6× (EE) gains	1

reliability [10]; MAPC/MLGP optimise back-haul routing under a deterministic topology [3]; IMCA resolves only the initial link-matching phase [11]; GAPC maximises spectral efficiency in isolation [13]; WNV-based association concentrates on virtual slicing without relaying [12]; energyaware sleep-control for heterogeneous 5G cells targets only power reduction, omitting outage and spectral aspects [14]; and ECM+BPSD focus on small-cell placement for energy saving, again without a joint QoS analysis [15]. None of these studies (i) quantifies outage probability, spectral and energy efficiency **jointly** under a stochastic-geometry (Thomas PCP) deployment, (ii) exposes the coverage-efficiency tradeoff created when hop count, cluster density, and SINR threshold are co-optimised, or (iii) reports the baselineto-UE-VBS performance delta in concrete figures that practitioners can reuse. First, we derive the first closed-form outage model for UE-VBS networks, validate it with LOGDfading simulations, and then couple it with new analytical expressions for system-wide spectral and energy efficiency that bind hop count, SINR threshold, and cluster-head probability. Second, we provide the first holistic comparison with legacy macro-cell operation under identical traffic and propagation assumptions-showing, for example, that at 2 UE/m<sup>2</sup> a single-hop slice cuts outage from 0.78 to 0.23 while boosting area-spectral efficiency by 4.8× and energy efficiency by 4.6×. Table 2 highlights how our framework extends or supersedes each representative line of research.

#### **III. ASSUMPTIONS RELATED TO SYSTEM FORMULATION**

To analyze our UE-VBS system, we have made some assumptions about signal processing, random properties, and the hardware being used. More specifically, we assumed a decentralized UE-to-VBS communication model where each UE can dynamically act as a Virtual Base Station (VBS) based on its proximity, available resources, and quality of the wireless link. All UEs and VBSs are equipped with single antennas, operate in full-duplex mode (leveraging recent demonstrations of >100 dB self-interference cancellation), and support D2D communication; Section V quantifies the  $\approx$ 50 % throughput reduction under a half-duplex constraint. We consider standard LTE/5G-compliant PHY and MAC layers with device capabilities constrained by finite-resolution DAC/ADC, non-ideal power amplifiers, and oscillator phase noise. The wireless channels are modeled as Rayleigh fading with distance-dependent path loss and log-normal shadowing. Perfect synchronization is assumed, while channel state information (CSI) may be imperfect. The decision of VBS selection and the clustering of UEs follow a semi-static configuration updated periodically based on traffic load and mobility patterns. Energy constraints are incorporated, especially for battery-operated UEs acting as VBSs. The below-mentioned assumptions are the most significant ones, whereas the less significant assumptions are mentioned as they come up in later sections.

#### A. UE-VBS RELAY FUNCTIONALITY

Firstly, we assume that the UE-VBS-enabled devices can function as relays in a full-duplex manner. This assumption is technologically grounded rather than speculative. Laboratory prototypes have already achieved > 100 dB self-interference cancellation on commodity smartphone chipsets at sub-6 GHz, enabling practical in-band full-duplex links [17], [18]. In parallel, 3GPP Release 18 introduces in-band full-duplex (IBFD) operation for 5G NR small-cell nodes, paving the way for handset vendors to expose the capability in upcoming devices. We therefore treat full-duplex UE-VBS relays as a realistic, forward-looking upper bound. Section V later quantifies how our results would scale down under a halfduplex constraint, showing that the qualitative conclusions remain intact despite the expected 50 % throughput reduction. Suppose we have a half-duplex relay communications; then Shannon-Hartley channel capacity would be decreased by a factor of  $\frac{1}{n}$ . This decrease in capacity is due to the split in the uplink and downlink channels in time and frequency. A full-duplex relay means that two antennas receive and transmit using the same frequency simultaneously, which causes high interference between them. Recently, there have been advancements in full-duplex relays [17], [19], [20] that deal with this interference in many different ways. The performance of the relay depends on the hardware with which the UE-VBS computing system can integrate itself. A decode and forward relay would be beneficial if sufficient buffer memory is available. Also, if we can decrease the interference



(actively or passively) below the noise level and utilize the same frequency band, we can realize a relay kind of setup. This assumption essentially falls onto the hardware/signal processing used during deployment.

#### B. MODELING OF UE SPECIAL 2D DISTRIBUTION

As discussed previously, we can describe the locations of set U on a 2D plane with the Thomas Clustering technique. We simulate random point generation representing UEs using R, specifying the initial PPP intensity  $(\lambda)$ , the variance  $(\sigma^2)$  of the 2D isotropic Gaussian clustering, and the average number of points  $(\lambda_c)$  within each cluster. This allows us to use these variables to create UE positions and densities akin to those of a busy city center in many European countries [7]. We use these U sets to generate UE-VBS networks by assigning devices as either  $U_{UE-VBSCH}$  and  $U_{AV-RL}$ . Finally, we draw randomly probable connections to the served devices from either the gNodeB (BS) or a device in  $U_{UE-VBS}$ . Thus, this investigation is focused only on the second dimension (2D) rather than the third dimension (3D).

# C. PROBABILITY FOR PRESENCE OF A UE-VBS DEVICE IN A CLUSTER

It is intuitively understood that only some clusters will have a UE-VBS-enabled device to serve them, as it is potentially a random event. These enabled devices are modeled as a random sample from the set of all devices U (which becomes  $U_{UE-VBS}$ ) in A. This random sample will extract a predetermined percentage of the devices, denoted by  $\mathbf{u}$ . Therefore, we can assume that each device will have a probability u to be chosen. Suppose we have an average number of devices in a cluster of  $\lambda_c$ , where a Binomial distribution is used to model the probability that each cluster will have at least one cluster head. This is accomplished via the subsequent equation.

$$p_p = Pr\{(n \ge 1 | \lambda_c), u\} = \sum_{n=1}^{\lambda_c} n \cdot u (1 - u)^{n-1}$$
 (3)

This probability distribution will be used in the later analysis to fully incorporate that not all clusters will have a  $U_{UE-VBS}_{CH}$  included (Section V-A).

In the UE-VBS paradigm, we assume that a fixed fraction u of all UEs in the cell have the special UE-VBS app installed and thus are eligible to act as cluster heads. Every such UE-VBS-capable device is automatically promoted to a cluster head. Under this random sampling, a cluster containing on average  $\lambda_c$  UEs will have at least one head with probability  $p_p$  (Eq. 3); If no head lands in a cluster (probability  $1 - p_p$ ), that cluster is deemed headless and is treated as a local outage.

#### 1) CLUSTER-HEAD SELECTION

Each UE  $i \in U$  is independently marked UE-VBS-capable with probability u, so that

$$U_{UE\text{-}VBS} = \big\{ i \in U \mid \Pr[i \in U_{UE\text{-}VBS}] = u \big\}.$$

By construction, every such UE-VBS-capable device becomes a cluster head, i.e.

$$U_{UE-VBSCH} = U_{UE-VBS}$$
.

Since a typical cluster contains  $\lambda_c$  UEs and each is chosen with probability u, the probability that *at least one* lies in that cluster is exactly

$$p_p = \sum_{n=1}^{\lambda_c} n u (1-u)^{n-1},$$

as given in Eq. (3). Any cluster that by chance has no head (probability  $1 - p_p$ ) is then treated as headless (i.e. instantaneous local outage).

# D. MULTIPLE ACCESS CHANNEL BASED ON ORTHOGONAL FREQUENCY DIVISION MULTIPLE ACCESS

It is noteworthy to add that because the application of this system is intended for implementation on contemporary 5G systems, we aim to use Orthogonal Frequency-Division Multiple Access (OFDMA) to access the various UE-VBS channels [21]. This dramatically decreases interference between the carriers and allows the proposed approach to model the system with "flat" fading, which means that the bandwidth of each sub-carrier is smaller than the coherence bandwidth. This lets us represent the model fading components in random wireless signals as a single RV.

Furthermore, additional resources, such as data rate and bandwidth, must be allocated to specific UE-VBS devices. These devices will be responsible for serving not only themselves but also a larger number of devices on certain occasions. OFDMA enables the allocation of several Orthogonal Frequency-Division Multiplexing (OFDM) subbands to adjust the data rate available to a specific UE device.

#### IV. SYSTEM MODELING AND FORMULATION

# A. GENERAL DESCRIPTION AND FORMULATION OF THE UE-VBS MODEL

Generally, our model will always either consist of one or more hops to form a UE-VBS cluster of devices or to act as a direct connection to a UE device. As the direct connection is standard, we will focus on the novel UE-VBS connection in our analysis (as shown in Fig. 3).

As seen in the signal model diagram in Fig. 3, a single spanning of a UE-VBS network would have n number of UE-VBS<sub>RL</sub> devices (or hops) connecting to a UE-VBS<sub>CH</sub> and k UE-client devices. Each link (arrow pointers in Fig. 1) shown can be described as a wireless signal travelling from device a to b and can be expressed as follows:

$$y_{a \to b}(t) = h_{a \to b}(t)x_{a \to b}(t) + n_b(t) \tag{4}$$

where  $h_{a\to b}(t)$  is the channel of multiplicative noise fading coefficient for the message  $x_{a\to b}(t)$ , and  $n_b(t)$  the Additive White Gaussian Noise (AWGN). We can extract useful parameters such as power, Signal-to-Noise Ratio (SNR), and Signal-to-Interference Ratio (SINR) from these signals.



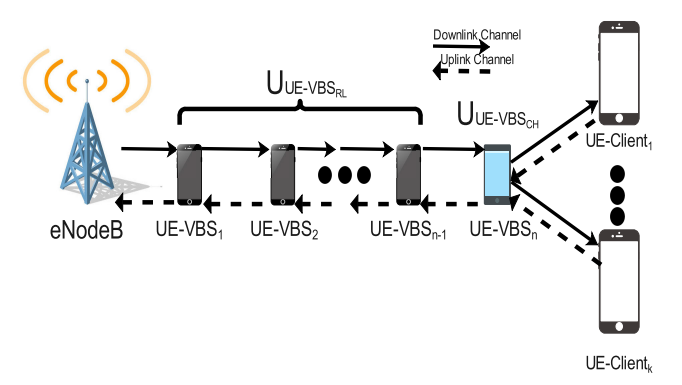


**FIGURE 3.** A signal model for a spanning tree connection in a UE-VBS network.

To analyze the system further, we need to convert the physical signal into a power signal. Using the FSPL Model as part of the link budgeting equation [22], non-logarithmically, we can say that power at b that is transmitted from a is given in the following equation.

$$P_b = \frac{P_a h_{a \to b} G}{l(r)} \tag{5}$$

where  $P_a$  and  $P_b$  are the instantaneous powers at arbitrary points a and b in our area of interest, l(r) is defined in Table 1, and G is the overall gain of the antennas. This can be described as  $G = G_t G_r$ , where  $G_t$  and  $G_r$  are the transmitter and receiver antennas gain, respectively.

Upon closer examination of our model, it becomes apparent that the signals depicted in Fig. 3 should not be regarded as equal. This is because the power, range, and channel properties of the connections can be categorized into three distinct stages, as outlined below.

- 1) Stage 1 gNodeB to first UE-VBS device: Initially, a BS or gNodeB will connect to a UE-VBS-enabled device in our generated network. Here, we can expect a higher initial transmission power in practice as this will usually be the longest distance our signal will travel (<1km). The channel here is expected to be affected by slow (Lognormal noise) and fast (Rayleigh noise) fading due to the multiple-path signals arriving at our receiver [23]. To simplify our analysis, we assume that all stages experience only Rayleigh fading and deterministic power loss.
- 2) Stage 2 UE-VBS multi-hop "bus": At this stage, we may have an arbitrary number of hops but will choose to limit this to a pre-determined number. The channels here are relayed by UE devices that are UE-VBS enabled (full-duplex manner) to reach a  $U_{UE-VBS}_{CH}$  device. The length of the 'chain' depends on where the cluster of devices we are trying to reach is located and the angle of incidence of  $U_{UE-VBS}$  devices along the way. Although the individual connections will be at a maximum of 500 m long due to limitations of Long Term Evolution (LTE) direct [24], it is expected that at this stage, we may experience a

power outage at most since low-powered UE devices are being used. A maximum of  $H_{\text{max}}$  relay hops is supported. This limit is not imposed by UE hardware alone but is a performance-driven design choice: more hops extend coverage into deeper fades, but each extra relay adds processing/queuing delay, increases aggregate interference, and incurs additional energy and signalling overhead. The per-hop distance remains bounded by the LTE-Direct range ( $\approx$  500 m) and full-duplex self-interference cancellation capabilities, while  $H_{\text{max}}$  itself is selected via empirical optimization to balance coverage, latency, spectral efficiency, and energy consumption. The  $H_{\text{max}}$  is set to 5, to capture diminishing returns beyond this point; hardware-level constraints inform the per-hop distance, but the hop count itself reflects a design trade-off to maximize userperceived QoS and network efficiency.

3) Stage 3 - UE-VBS cluster head to cluster devices:

The final stage, which is used to serve the multiple devices of the cluster, will be a multiple access channel that will provide a downlink data signal to the UE devices. Furthermore, in order not to have a 'bottleneck' for the data rate, we must provide an expanded bandwidth for this particular spanning tree collection, depending on the number of devices expected to be served, and hence a higher possible data rate to accommodate the requirements of all devices. This is made possible by allocating more sub-carriers from the OFDMA system for these connections, starting from the first device in stage 1.

#### a: PATH LOSS MODEL IN ANALYTICAL RESULTS

In the analytical model, we assume a free-space path loss model, which describes how signal strength diminishes purely as a function of distance in a free-space environment without obstructions. The SNR is computed under the influence of AWGN, which accounts for random noise in the communication channel.

#### **B. OUTAGE BEHAVIOR**

As mentioned in the previous section, there is a difference in how we should treat the three stages. In our study, we assume that a device is considered to be in an outage if its SINR falls below a specified threshold  $SINR_{TH}$ . The FSPL Model estimates the signal power attenuation. Thus, the outage probability is given by  $Pr\{SINR < SINR_{TH}\}$ , as shown in Eq. (17).

Notably, the upper bound of  $SINR_{TH}$  can be determined by adjusting  $R_{min}$  in the modified Shannon capacity equation for noisy channels [25], which is given by the following equation.

$$2^{\frac{R_{\min}}{BUE - VBS}} - 1 = SINR_{TH} \tag{6}$$

where  $B_{UE-VBS}$  is the bandwidth allocated for individual UE-VBS spanning tree channel connections. Now, we can join all three stages to calculate the outage probability for



the end-to-end connection. Intuitively, we can see that if one connection drops, the connections to all stages drop. So, in a 'chain-like' fashion, the Eq. (7) can be utilised.

$$P_{OutD} = 1 - (1 - p_{out,init})(1 - p_{out,UE-VBS})(1 - p_{outC})$$
(7)

where  $p_{out,init}$ ,  $p_{out,UE-VBS}$  and  $p_{outC}$  are the outage probabilities for the initial gNodeB to first UE-VBS device stage, the middle multi-hop "bus" and the final clustering stage, respectively.

#### C. LOGD PATH LOSS MODEL EXAMINATION

Wireless communication systems rely heavily on accurate models to predict path loss across different environments. The practicality of path loss models is crucial for designing efficient communication networks by estimating the attenuation of signals as they propagate from a transmitter to a receiver. With its adaptability and precision, the Log-Distance (LOGD) path loss model with shadowing effects is a theoretical construct and practical tool that can be readily applied in various scenarios. This section introduces and details these two models, providing insights into their formulations and real-world applications. The LOGD path loss model, also known as the LOGD power law model, is a simple yet effective model used to predict the path loss encountered over a distance in wireless communication systems. It is a generalization of the FSPL model and is widely used due to its simplicity and adaptability to different environments by tuning its parameters.

#### a: FORMULATION

The LOGD path loss model is mathematically expressed as:

$$PL(d) = PL(d_0) + 10 \cdot \alpha \log_{10} \left(\frac{d}{d_0}\right) + X_\sigma, \quad (8)$$

where:

- PL(d) is the path loss at distance d in dB,
- $PL(d_0)$  is the path loss at the reference distance  $d_0$  in dB,
- α is the path loss exponent, indicating how path loss increases with distance,
- d is the transmitter-receiver separation distance,
- d<sub>0</sub> is a reference distance from the transmitter within the far-field region,
- X<sub>σ</sub> is a Gaussian random variable (in dB) representing shadowing effects, with zero mean and standard deviation σ.

#### b: APPLICATION

The LOGD path loss model is extensively used in both outdoor and indoor scenarios for its flexibility and simplicity. By adjusting the path loss exponent n and the shadowing deviation  $\sigma$ , the model can be tailored to fit a wide range of environments, from urban to rural and from indoor office spaces to industrial settings. This model is particularly valuable in the initial stages of network design

and simulation, providing a reliable basis for estimating the coverage and capacity of wireless communication systems.

#### D. THROUGHPUT AND EFFICIENCY

Next, spectral and energy efficiency are examined in our investigation. As the system's main resources will be the frequency spectrum and power, quantification of these values must occur in the future to optimize the system as much as possible. The data rate R in the system can be defined using Shannon's capacity formula, which is a function of the system's bandwidth B and the signal-to-interference-plusnoise ratio SINR. The data rate R is expressed as:

$$R = B\log_2(1 + SINR) \tag{9}$$

Continuing, the total system bandwidth, denoted as  $B_{sys}$ , represents the entire frequency spectrum allocated for the system. It is shared among multiple users or connections, influencing both the spectral and energy efficiency of the system. The total bandwidth available for all UE-VBS connections and users within the system is given by:

$$B_{sys} = \sum_{i=1}^{n} B_i \tag{10}$$

where  $B_i$  is the bandwidth allocated to the *i*-th user or connection, and *n* is the total number of users or connections. The total bandwidth is normalized by  $B_{sys}$  when calculating spectral efficiency.

#### 1) SPECTRAL EFFICIENCY

To analyze the stochastic geometrical distribution of UE devices, it is essential to assess the spectral efficiency over the expected coverage area. The spectral efficiency  $\eta_{\text{sysSE}}$ , where  $\eta_{\text{sysSE}}$  represents the system's spectral efficiency, can be calculated as shown:

$$\eta_{\text{sysSE}} = \frac{\eta_{all-linkSE}}{A} \tag{11}$$

where  $\eta_{all-linkSE}$  is the predicted capacity of all UE-VBS connections and A is the expected coverage area of the cell used.

If AWGN power can be represented as  $W = N_0 B_{UE-VBS}$ , where  $N_0$  is the power spectral density of the noise, we can then represent the instantaneous capacity of a link using the Shannon noisy channel equation  $C_1 = Blog_2(1 + \frac{P_1G_1h_1d_1^{-\alpha}}{W+I})$  [bits/s]. The ergodic capacity of a fading channel is calculated by taking the expected value of the channel capacity, assuming Rayleigh fading RV [26] as shown below.

$$C_{1} = E \left\{ B \log_{2} \left( 1 + \frac{P_{1}G_{1}h_{1}d_{1}^{-\alpha}}{W+I} \right) | h \right\}$$

$$= \int_{0}^{\infty} B \log_{2} \left( 1 + \frac{P_{1}G_{1}h_{1}d_{1}^{-\alpha}}{W+I} \right) dF_{H}(h)$$
 (12)

where  $F_H(h)$  is the CDF of the Rayleigh fading RV or, more generally, the SINR. It is essential to point out that B here would be  $B_{SVS}$  divided by the number of devices in



the network, assuming an equal data rate for all of the UEs in the network. From here, we can formulate an equation describing  $\eta_{all-linkSE}$  for all of our connections. If a UE device is directly connected to the BS, then its capacity can be described as explained above. However, if we have a spanning tree connection, as shown in Fig. 3, and if we wish to allocate the same amount of bandwidth to all of the tree's connections, we need to account for the relay bus and the cluster. Consequently, the link capacities' sum can be shown below.

elow.  

$$\eta_{\text{all-linkSE}} = \frac{\sum_{i=1}^{u} C_i + \sum_{z=1}^{t} \left( \sum_{q=1}^{n_{rz}} C_q + \sum_{m=1}^{n_{cz}} C_m \right)}{B_{\text{sys}}}$$

$$= \frac{R}{B_{\text{sys}}} \tag{13}$$

where u is the number of UE devices connected directly to the gNodeB, t is the number of spanning trees,  $B_{sys}$  is the total bandwidth used by the 5G system,  $n_{r_z}$  and  $n_{c_z}$  are the number of relay and cluster devices in the tree, respectively. Furthermore, R gives our system's expected upper bound of the data rate.

#### 2) ENERGY EFFICIENCY

Optimizing energy efficiency in modern 5G/6G systems is necessary due to the significant societal and economic concerns associated with increased power usage. To extract our system's minimum acceptable energy efficiency, we need to quantify how much power is being used instantaneously by the system for a minimum required throughput (as shown in Eq. (14)). Thus, energy efficiency is calculated using the following equation:

$$\eta_{sysEE} = \frac{R_{\min}}{P_{tot}} \tag{14}$$

where  $P_{tot}$  is the total instantaneous power being used. More specifically, this power can be split into two distinct parts. The power being actively used to transmit messages, which is  $P_t = \sum_{i=1}^{u} P_i + \sum_{z=1}^{t} \left(\sum_{q=1}^{n_{rz}} P_q + \sum_{m=1}^{n_{cz}} P_m\right)$ . Note that the gain G from Eq. (5) in each transmission will be accounted for by introducing an average power loss factor  $\beta$  to all transmitted power signals  $(P_t)$ , which will be an average power cost for all gains in our system. The other aspect of power usage is determined by the hardware in the transmitters and receivers that are needed to keep the connections live. This can be described by a constant power loss  $P_c$  and a dynamic power loss  $P_c$  that depends on  $P_t$  so, we can say that  $P_{tot}$  can be calculated as in the following equation:

$$P_{tot} = \beta P_t + P_c + \gamma R_{\min} \tag{15}$$

Other than providing a consistently high QoS, the primary goal is to optimize and balance energy and spectral efficiencies through suitable optimization methods. Eq. (16) formulates this optimization problem by defining the system energy efficiency  $\eta_{sysEE}$  as the ratio of the minimum required

throughput  $R_{\min}$  (ensuring that QoS remains constant) to the overall effective power consumption, which is given by  $\beta P_t + P_c + \gamma R_{\min}$ . Here,  $P_t$  represents the transmission power bounded within  $[P_{t_{\min}}, P_{t_{\max}}]$ ,  $P_c$  denotes the constant circuit power consumption, and  $\gamma$  is a non-negative parameter that accounts for additional costs proportional to  $R_{\min}$ . The constraints in the optimization problem ensure that  $R_{\min}$  is non-negative, the transmission power  $P_t$  remains within its prescribed limits, and  $\gamma$  is also non-negative. Overall, this formulation encapsulates the trade-off between maintaining a minimum throughput for QoS and minimizing the effective power consumption to achieve optimal energy and spectral efficiency.

$$\max_{\eta_{sys}EE} \quad \left\{ \eta_{sys}EE} = \frac{R_{\min}}{\beta P_t + P_c + \gamma R_{\min}} \right\}$$
subject to: 
$$R_{\min} \ge 0$$

$$P_t \in [P_{t_{\min}}, P_{t_{\max}}]$$

$$\gamma \ge 0 \tag{16}$$

#### 3) ON THE OPTIMIZATION OF THE EFFICIENCIES

Through further inspection of  $\eta_{sysSE}$  and  $\eta_{sysSE}$  and according to Eq. (13), we can gain knowledge on what values we need to optimize specifically.  $\beta$  and  $\gamma$  are also constants due to the dependency on hardware. The values that are left are  $P_t$  and  $P_c$ . While  $P_c$  is a constant itself, it does have a connection to how many devices are being utilised in the system, so we can say that  $P_c \propto nP_{ue}$ , where n is the total number of devices in the UE-VBS network, and  $P_{ue}$  is the average power usage per device. Now, we can also see that  $P_t$  heavily depends on the number of devices n as well.

We assume that the power allocated for each transmission in our system is directly affected by the expected reach of the transmission. Therefore, it is evident that shorter transmissions would decrease  $P_t$ . To be specific, short transmissions take place inside the spanning trees, i.e., UE-VBS<sub>1</sub> to UE-Client<sub>m</sub>, where l and m are randomly selected from the set of the available VBS, and UEs devices, respectively, and hence, higher the number of trees t (i.e. more relays), we may see an increase in  $\eta_{sysEE}$ .

Therefore, we optimize the system by obtaining values allowing for the highest efficiencies. Both  $\eta_{sysEE}$  and  $\eta_{sysSE}$  need to be taken into consideration so that it can be shown that our analysis is well suited for real-world applications. Several methods can be employed to optimize the abovementioned parameters, which will be discussed in the forthcoming discourse.

#### **V. ANALYSIS**

This section uses the AWGN model to explore the system's performance metrics, examining outage probability, spectral efficiency, and energy efficiency. The analysis segments the network into different operational stages to evaluate each link in the communication chain.



#### A. OUTAGE PROBABILITY

To effectively assess the coverage and performance of our system, we investigate the probabilistic behavior of the downlink power signals from each device in the spanning tree. Hence, we intuitively split Fig. 3 into three distinct parts:

1) eNodeB to first UE-VBS device: For the sake of simplicity, we can either ignore fast fading or use the link budgeting equation to analyze the probability that the power loss is higher than a specific acceptable limit. However, in our case, we ignore power loss and shadowing and use the convenient Rayleigh distribution [22], which has an SNR distribution of  $p_{RP}(x) = \frac{1}{SNR}e^{-\frac{x}{SNR}}$  [27]. It is worth noting that for this stage, we assume that SNR = SINR allows for the use of the SNR PDF. The impact of this assumption is believed to be minor due to the much greater transmission power that gNodeB will be transmitting when compared to the interference added. Therefore, the probability (the outage probability) that the SINR will be below a specific limit can be expressed as shown in the following equation:

$$p_{\text{out,init}} = Pr \{ \text{SINR} < \text{SINR}_{\text{TH}} \}$$

$$= \int_{0}^{\text{SINR}_{\text{TH}}} p_{\text{RP}}(x) dx$$

$$= 1 - \exp\left(-\frac{\text{SINR}_{\text{TH}}}{\text{SINR}}\right)$$
(17)

2) **UE-VBS multi-hop "bus":** Given our assumptions in Section III, we can say that our potential transmitters can be assumed to be located at the center of the Poisson distributed clusters. From the relevant literature [6], it can be stated that the Laplace transform of the interference is equal to the probability of coverage (the probabilistic opposite of outage), which is given by the following equation. So, the probability of signal coverage at a specific point *i* in a network, denoted by  $P_{s.i.}$ , is defined by:

$$P_{s,i} = \Pr\{SIR > SIR_{TH}\}\$$

$$= \exp\left(-c_d \lambda SIR_{TH}^{\delta} r_i^d \Gamma (1-\delta)^2\right)$$
(18)

Where  $c_d$  represents the area over which User Equipment is spread out, reflecting the spatial distribution of transmitters. The parameter  $\lambda$  refers to a density factor associated with the Poisson distribution of transmitter clusters, indicative of how densely packed these potential transmitters are within the defined area. The variable  $r_i$  represents the average one-hop distance to the ith point or node in the network, and  $\Gamma(.)$  denotes the Gamma function, a generalization of the factorial function that accommodates complex and real number arguments. Additionally,  $\delta = \frac{d}{a}$  is a dimensionless parameter linking the dimension d of the environment to the path loss factor a. d is the dimensionality (specifically 2 in this two-dimensional scenario), and a

is the path loss exponent that characterises how rapidly the signal power decreases with distance, chosen here as 4 for convenient calculation. So, SIR represents the Signal-to-Interference Ratio, measuring signal quality by comparing the power of the signal to the power of the background interference.  $SIR_{TH}$  is the threshold level above which the signal is considered to be in "coverage," thus determining whether the SIR at point i exceeds this threshold. The formula under discussion calculates the probability of coverage in a wireless network, particularly focusing on the scenario where the Signal-to-Interference Ratio (SIR) surpasses a specified threshold  $SIR_{TH}$ . This is vital for assessing the performance and reliability of communications in UE-VBS multi-hop networks. The formula's core principle is to model the likelihood of adequate signal coverage at a given network point, considering how interference impacts signal quality and communication reliability. It highlights that increasing interference,  $SIR_{TH}$ ,  $\lambda$  (the density of transmitters), or  $r_i$  (average distance to the ith node) escalates the exponent in the exponential term, consequently reducing coverage probability. Note that in the original equation, the  $r_i$  is defined with  $r_d$ , and d is the dimension. The assumption that transmitters are centrally located within Poisson-distributed clusters reflects a realistic spatial node distribution, influencing interference and coverage outcomes. Additionally, the parameter  $\delta$ , representing the ratio of spatial dimension to path loss factor, adjusts the model to account for distance-based signal power decay, thus providing insights into the environmental effects on signal propagation and interference. Ultimately, the formulation shown in Eq. (19) estimates the likelihood of maintaining adequate signal quality above a specific threshold in a UE-VBS multihop network, factoring in node distribution, inter-node distances, and environmental characteristics.

Thus, by having the given expression for the probability of signal coverage is:

$$P_{s,i} = \exp\left(-c_d \lambda SIR_{TH}^{\delta} r_i^d \Gamma(1-\delta)^2\right)$$
 (19)

where:

- c<sub>d</sub> is a coefficient related to the coverage area,
- $\lambda$  is the density of transmitters,
- SIR<sub>TH</sub> is the signal-to-interference threshold,
- $\delta$  is defined as  $\frac{d}{a}$ ,
- $r_i$  is the average distance to the *i*th node,
- $\Gamma(1-\delta)$  is the Gamma function evaluated at  $1-\delta$ .

Given that  $\delta = \frac{d}{a}$ , and substituting d=2 and a=4 (the dimensional and loss factors respectively), then  $\delta = \frac{2}{4} = \frac{1}{2}$ , Substituting  $\delta = \frac{1}{2}$  into the original equation, we obtain:

$$P_{s,i} = \exp\left(-c_d \lambda SIR_{TH}^{\frac{1}{2}} r_i^2 \Gamma\left(1 - \frac{1}{2}\right)^2\right)$$
 (20)



The Gamma function  $\Gamma(1-\delta)$  with  $\delta=\frac{1}{2}$  simplifies to  $\Gamma\left(\frac{1}{2}\right)=\sqrt{\pi}$  Therefore,  $\Gamma\left(\frac{1}{2}\right)^2=\pi$ . The final expression for the probability by substituting

 $\delta = \frac{d}{a}$ , where d is 2 and a is 4, the result simplifies to:

$$P_{s,i} = \exp\left(-c_d \lambda SIR_{TH}^{\frac{1}{2}} r_i^2 \pi\right)$$
 (21)

which reflects how environmental changes and signal characteristics impact the coverage probability. This formula effectively captures how the likelihood of maintaining a signal strength above a certain threshold decreases as the interference increases.

More precisely, to derive Eq. (21) we proceed in the following step by step examination:

$$P_{s,i} = \exp(-c_d \lambda \operatorname{SIR}_{TH}^{\delta} r_i^d \Gamma(1-\delta)^2).$$

- $c_d$  is the unit-ball area in d dimensions [6],
- $\lambda$  is the density of transmitters,
- SIR<sub>TH</sub> is the SIR threshold,
- $\delta = d/a$  is the ratio of dimension to path-loss
- r<sub>i</sub> is the link distance,
- $\Gamma(1-\delta)$  comes from the Rayleigh-fading Laplace transform.

1. In our urban NLOS scenario we set d = 2 and a = 4,

$$\delta = \frac{d}{a} = \frac{2}{4} = \frac{1}{2},$$

and hence  $SIR_{TH}^{\delta} = SIR_{TH}^{1/2}$  [7].

2. Using  $\Gamma(\frac{1}{2}) = \sqrt{\pi}$  [28, Ch. 6], we get

$$\Gamma(1-\delta)^2 = \pi.$$

- 3. In two dimensions the unit-disk area is  $c_d = \pi$  [6].
- 4. Substituting  $\delta = \frac{1}{2}$ ,  $\Gamma(1 \delta)^2 = \pi$ , and  $c_d = \pi$  into the exponent yields

$$P_{s,i} = \exp\left(-\pi \lambda \operatorname{SIR}_{TH}^{\frac{1}{2}} r_i^2 \pi\right)$$
$$= \exp\left(-c_d \lambda \operatorname{SIR}_{TH}^{\frac{1}{2}} r_i^2 \pi\right).$$

Thus we recover

$$P_{s,i} = \exp\left(-c_d \lambda \operatorname{SIR}_{TH}^{\frac{1}{2}} r_i^2 \pi\right),\,$$

which shows coverage probability decays exponentially in  $\lambda$ ,  $r_i^2$ ,  $SIR_{TH}^{1/2}$ , and  $\pi$ .

More specifically, to continue our investigation by having  $\delta = \frac{d}{a}$ , where d is the dimension we have in our environment (2 in our case), and a is the loss factor, which is chosen to be 4 to allow for the convenient calculation seen in Eq. (22). Thus, the result is  $\exp(-c_d \lambda SIR_{TH}^{\frac{1}{2}} r_i^2)$ . It would be worth noting that

we assume Rayleigh fading<sup>2</sup> with mode one<sup>3</sup> [29], to keep our solution simple. As we also want to account for additive noise in our analysis, we use a modified version of Eq. (18), which takes the following form of Eq. (22). Note that W denotes the Additive White Gaussian Noise, and this term is used to characterise the impact of noise on the probability  $P_{s,i}$ . For the transition of Eq. (18) to 22, involving SINR and noise W, we consider that the SIR to SINR transition can be measured as  $SINR = \frac{SIR}{1+W}$ , where W is the noise. If we incorporate the noise W into  $P_{s,i}$  using the relationship above, the exponent may be modified. However, the exact nature of this modification would depend on the specifics of your system model. The function  $\Gamma(1-\delta)\Gamma(1-\delta)$  could be a representation of some interference or fading effect. Rayleigh fading with mode one might be characterized by this term. If noise is being considered, the system may be simplified, leading to dropping or modifying this term. Given the information about Rayleigh fading and noise W, a simplified or approximate form by removing  $\delta$  could lead to Eq. (22). Typically, in communication systems, noise deteriorates the signal quality, affecting the reception or decoding of that signal. In the context of this equation, the presence of W inside the exponential function implies that as noise increases, the value of  $P_{s,i}$  decreases (given that other terms remain constant). To transition from the equation  $\exp(-c_d \lambda SIR_{TH}^{\frac{1}{2}}r_i^2\pi)$  to  $\exp(-SINR_{TH}r_i^2W)p_p$  using the relationship  $SINR = \frac{SIR}{1+W}$ , where W represents the noise, we need to undertake the following steps: The Initial equation is:

- a)  $\exp(-c_d \lambda SIR_{TH}^{\frac{1}{2}}r_i^2\pi)$  where:  $c_d$  is the area where User Equipment (U) is spread out,  $\lambda$  is a density parameter associated with the Poisson distribution of transmitter clusters,  $r_i$  is the average distance to the ith point or node in the network, and SIR<sub>TH</sub> is the threshold level for the Signal-to-Interference Ratio (SIR).
- b) Using the definition  $SINR = \frac{SIR}{1+W}$ , and substituting SIR in terms of SINR, we have: SIR = SINR. (1+W). This modification reflects the impact of noise on the system's performance, adjusting the SIR based on the noise level W.

<sup>2</sup>Rayleigh fading is a statistical model for the effect of a propagation environment on a radio signal, such as that experienced by mobile phones and wireless networks. It models the variation in amplitude of a signal received at a base station, which results from the many paths that a transmitted signal can take before being received. "Mode one" in Rayleigh fading typically refers to the simplest form of this fading model where the amplitude of the signal is modeled as a Rayleigh distribution, which is applicable when there is no line-of-sight path between the transmitter and receiver.

<sup>3</sup>Rayleigh fading with mode one assumes a non-line-of-sight (NLOS) propagation environment where multiple scattered paths contribute to the signal amplitude observed at the receiver. This model is characterized by its Rayleigh distribution of the signal's envelope, suitable for describing urban cellular radio and other similar environments where a direct visual path between transmitter and receiver is obstructed.



Modifying the Equation:

- a) To integrate the SINR into the initial equation, replace  $SIR_{TH}$  with its equivalent in terms of  $SINR_{TH}$ :  $SIR_{TH} = SINR_{TH} \cdot (1 + W)$ .
- b) Assuming W is small compared to 1, we can approximate 1 + W by W when it multiplies another large variable or is in an exponent. Then:  $SIR_{TH}^{\frac{1}{2}} \approx (SINR_{TH}W)^{\frac{1}{2}}$ .
- c) Substituting this into the original expression:  $\exp(-c_d \lambda (SINR_{TH}W)^{\frac{1}{2}}r_i^2\pi)$ .
- d) Assuming that the exponential and polynomial interactions allow a simplified model and recognizing that actual coverage probability might also include a probabilistic component  $p_p$  (reflecting other system aspects like probabilistic distribution of nodes, as shown in Section III-C), we approximate:  $\exp(-SINR_{\rm TH}r_i^2W)p_p$ .

Given the information about Rayleigh fading and noise W, a simplified or approximate form by removing  $\delta$  could lead to Eq. (22). Overall, in communication systems, noise typically deteriorates the signal quality, affecting the reception or decoding of that signal. In the context of this equation, the presence of W inside the exponential function implies that as noise increases, the value of  $P_{s,i}$  decreases (given that other terms remain constant). Also, it would be worth noting that we assume Rayleigh is fading with mode one to keep our solution simple. As we also want to account for additive noise in our analysis, we use a modified version of Eq. (18), which takes the following form:

$$P_{s,i} = \exp(-SINR_{TH}r_i^{\delta \cdot a}W)p_p$$
  
=  $\exp(-SINR_{TH}r_i^2W)p_p$  (22)

Note that W denotes the Additive White Gaussian noise, and this term is used to characterise the impact of noise on the probability  $P_{s,i}$ . For the transition of Eqs. 15 to 16, involving SINR and noise W, we can make a few considerations and hypotheses:

- SIR to SINR transition measured as:  $SINR = \frac{SIR}{1+W}$ , Where *W* is the noise.
- Accounting for Noise in  $P_{s,i}$ : If we incorporate the noise W into  $P_{s,i}$  using the relationship above, the exponent may be modified. However, the exact nature of this modification would depend on the specifics of your system model.
- Gamma Function: The function Γ(1 δ)Γ(1 δ)
   could be a representation of some interference
   or fading effect. Rayleigh fading with mode one
   might be characterized by this term. If noise is
   being considered, the system may be simplified,
   leading to dropping or modifying this term.
- The factor p<sub>p</sub> can be thought of as incorporating the probabilistic nature of having a transmitter within a particular range or the effect of other variables not explicitly modeled by the simplified SINR and

noise expressions. More specifically,  $p_p$  captures the likelihood that a UE-VBS-enabled device is present within a cluster, a random event. Devices enabled for UE-VBS are randomly selected from the set U (now  $U_{UE-VBS}$ ) in A, with each device having a selection probability u. Given an average  $\lambda_c$  devices per cluster, the probability that a cluster includes at least one cluster head is modeled using a Binomial distribution, as detailed in Equation 3.

This transition involves some approximations, particularly about the impacts of W and how it interacts with other variables in the system. The exact nature of these approximations should be validated by empirical data or more detailed analytical modeling to ensure that they accurately reflect the system's behavior under realistic operational conditions.

After calculating the outage for each link in the 'bus', the outages are combined and utilised with Eq. (3) to determine the probability that none of the links experiences an outage. In this context,  $P_{out,UE-VBS}$  can be expressed as:

$$P_{out,UE-VBS} = 1 - \prod_{i=1}^{n-1} (1 - P_{s,i})$$
 (23)

Here, the product  $\prod_{i=1}^{n-1} (1 - P_{s,i})$  represents the probability that all links in the "bus" are successful (i.e., none is in an outage). Thus, subtracting this product from 1 gives the overall probability that at least one link is in the outage, which is  $P_{out,UE-VBS}$ .

3) **UE-VBS** cluster head to cluster devices: The final stage of coverage for the devices included in the set S is very similar to the previous stage. However, the only difference in the calculation is that we only have a single stage and don't need to consider the probability of a transmitter existing in the cluster, as it has been considered in the previous stage. Therefore, we only need to use  $p_{outC} = 1 - P_{s,m}$  from Eq. (23) and adapt it to our average cluster parameters  $c_d$  and r.

We may apply the Eqs.  $\{(1) \text{ to } (4)\}$ . for the different stages along with Eq. (7) and vary  $\lambda$  to determine the outage for various numbers of devices in the cell (as shown in Fig. 4).

To determine the outage, we must first estimate the average distances each channel covers. From the structure of the network generated, it is noticed that in a network with only one hop being allowed, the initial distance (**eNodeB to first UE-VBS device**) is always around 0.9 km as the rest of the UE users are served directly by the cell tower (eNodeB). Hence, we use this distance in our analysis. Additionally, we have to choose a realistic value of  $R_{\rm min}$  and  $B_{UE-VBS}$  per channel, which is calculated empirically using data rate formulas and found in the open literature to be 300kbps and 1KHz, respectively [30], [31] in a specific low-data-rate application.



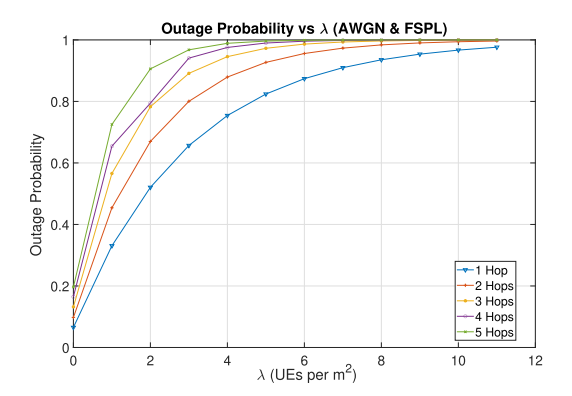


FIGURE 4. Outage analysis for UE-VBS networks with 1 to 5 hops to the cluster.

#### B. SPECTRAL EFFICIENCY

To analyze the spectral efficiency as shown in Fig 5, we need to obtain the statistical model of the SINR. Suppose that all devices require the same amount of content(data); analytically, the upper bound for area spectral efficiency for a Poisson distributed device system, such as the one considered in this work, can be approximated using Eq. (24) [31], [32]:

$$\eta_{\text{sysSE}} = \lambda \lambda_c \log_2(1 + \text{SINR})(1 - P_{\text{out}})$$
(24)

In this equation,  $\lambda \lambda_c$  represents the effective density of devices, while  $\log_2(1 + \text{SINR})$  gives the spectral efficiency of a single link. Multiplying by  $(1 - P_{\text{out}})$  accounts for the probability that a link is not in the outage, yielding an analytical upper bound for the area spectral efficiency of a Poisson distributed device system.

Also, it is possible to obtain an average spectral efficiency by using the expected values of all RVs in the SINR equation. As we have  $SINR = \frac{P_1G_1h_1d_1^{-\alpha}}{W+I}$ , and if we assume that  $G_1$  is unity for all transmitters, then we can use the mean values for  $I\{Interference\}$ . Consequently, the expectation can be expressed as follows:

$$E\{I\} = \pi \lambda + \frac{2\pi \lambda}{a - 2} (1 - R^{2-a}), \text{ for all } a > 0$$
 (25)

In this expression,  $E\{I\}$  denotes the expected interference. The first term,  $\pi\lambda$ , captures a basic interference contribution based on the device density  $\lambda$ . The second term,  $\frac{2\pi\lambda}{a-2}\left(1-R^{2-a}\right)$ , accounts for the effect of the path loss exponent a and the link distance R, and is valid for all values of a>0. This derivation assumes that  $G_1=1$  for all transmitters and uses the mean values for the interference.

#### C. ENERGY EFFICIENCY

We can also obtain the analytical expression for energy efficiency results similar to spectral efficiency, as shown in Fig. 6. The general energy efficiency is given in Eq. (16), and the maximum data rate is  $R = B\eta_{\text{sysSE}}$ , where B is a mean bandwidth as seen by our network, 1 KHz in our case. We can say that the analytical  $P_{tot}$  will constitute all of the initial power used to transmit through all links. Since our

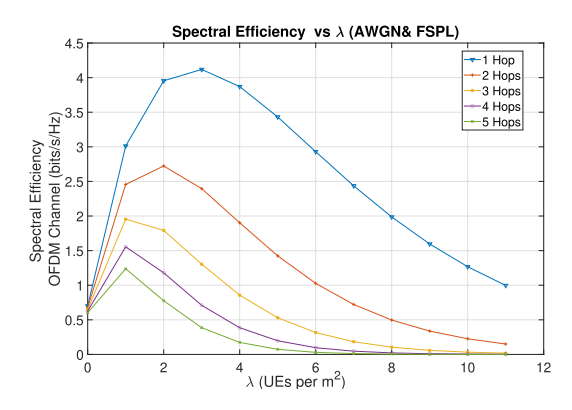


FIGURE 5. Spectral efficiency analysis results for UE-VBS networks with 1 to 5 hops to the cluster.

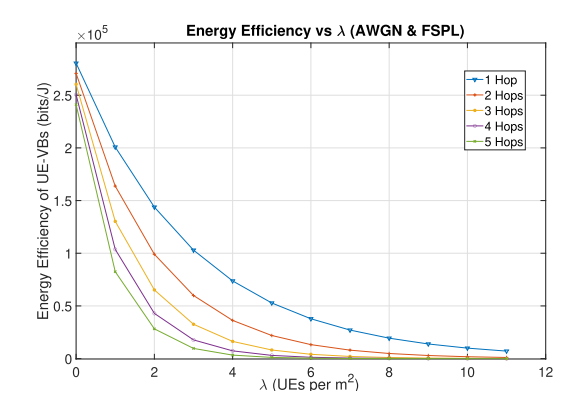


FIGURE 6. Energy efficiency analysis results for UE-VBS networks with 1 to 5 hops to the cluster.

power and gain are unity, we can obtain an average with  $P_{tot} = \lambda \lambda_c$ . Therefore, when we combine this observation, energy efficiency can be expressed analytically as shown in the following equation:

$$\eta_{sysEE} = \frac{B\lambda\lambda_c log_2(1 + SINR)(1 - P_{\text{out}})}{\lambda\lambda_c}$$

$$= Blog_2(1 + SINR)(1 - P_{\text{out}})$$
 (26)

In the next section, we verify the obtained analytical results with the aid of a simulation that imitates our system modeling presented in Section III.

#### VI. NUMERICAL SIMULATION

In this section, we indicate the simulation procedure and parameters. Moreover, we introduce our simulation model, which allows us to thoroughly examine the precision of the analytical model discussed in the previous section. Firstly, we create a process to automatically generate the random UE-VBS computing Infrastructures/networks with variable random intensities and settings (distances and a maximum number of devices). The generated infrastructures/networks are used as topological "frameworks" to assess their performance with randomly generated power signals. The networks' objects are generated through a brute force algorithm that uses randomly generated clusters



(U), on which the stem and cluster connections of the individual spanning tree networks are created. The developed frameworks are depicted in Fig. 7.

#### 1) SIMULATION PROCEDURE AND PARAMETERS

This subsection outlines the step-by-step workflow we follow for each simulation run: from random UE-VBS topology generation, through relay-tree construction and channel realization, to per-link SINR computation, outage/efficiency metric extraction, and finally ensemble averaging over 20 (or 150) independent trials.

Each data point is obtained by the following steps for a given  $\lambda$ :

#### 1) Topology generation.

- Scatter "parent" points over the 1 km×1 km area via a PPP(λ).
- For each parent, draw  $Pois(\lambda_c)$  "children" with isotropic Gaussian spread  $\sigma$ .
- Mark each child UE as VBS-capable with probability *u*.

#### 2) Tree construction.

- For every VBS-capable UE, form a relay tree up to  $H_{\rm max}$  hops, respecting per-hop distances  $d_{BS}^{\rm max}$ ,  $d_{RL}^{\rm max}$ ,  $d_{CH}^{\rm max}$ .
- Attach any remaining UEs within  $d_{CH}^{\text{max}}$  of a cluster-head as clients.

#### 3) Channel realization.

- Compute link path loss:
  - FSPL regime: exponent = 2, no shadowing.
  - LOGD regime: exponent =  $\alpha$ , shadowing  $\mathcal{N}(0, \sigma_{shad}^2)$ .
- Generate Rayleigh fading gains; sum interference from all simultaneously active transmitters (LOGD only).
- Add AWGN with density  $N_0$ .

#### 4) Metric computation.

- Per-link SINR  $\rightarrow$  outage if below SINR<sub>TH</sub> (Eq. (6)).
- Aggregate end-to-end outage (Eq. (7)).
- Compute spectral and energy efficiency via Eqs. (10)–(13).
- 5) **Averaging.** Repeat 20 realizations for outage curves; 150 for efficiency plots; report the ensemble mean.

Table 3 collects every numerical constant that shapes the synthetic deployments and the performance plots. A square macro-cell of 1 km  $\times$  1 km (A) is filled by a Thomas Poisson-cluster process whose parent intensity  $\lambda$  is swept from 0.5 to 12 UEs m<sup>-2</sup> in 0.5 steps; each parent spawns, on average,  $\lambda_c = 10$  children drawn from a bivariate normal with standard deviation  $\sigma = 30$  m. Each child is promoted to a UE-VBS candidate with probability u = 0.25, after which the topology solver grows relay trees of up to  $H_{\rm max} \in \{0,\ldots,5\}$  hops while honouring the reach limits  $d_{\rm BS}^{\rm max} = 900$  m,  $d_{\rm RL}^{\rm max} = 500$  m and  $d_{\rm CH}^{\rm cm} = 50$  m.

**TABLE 3.** Unified list of simulation parameters.

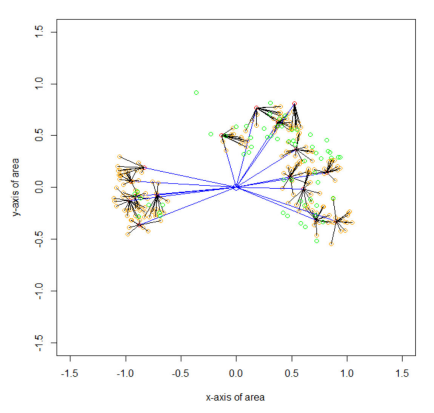
Symbol / item	Meaning	Value
	Topology	
A	Square-cell dimensions	$1000 \mathrm{m} \times 1000 \mathrm{m}$
$\lambda$	Parent-PPP intensity (sweep)	0.5:0.5:12 UEs m <sup>-2</sup>
$\lambda_c$	Mean UEs per cluster	10
$\sigma$	Cluster standard deviation	30 m
u	UE-VBS selection probability	0.25
$H_{ m max}$	Hop cap. $\{0,, 5\}$	see figures
$d_{\rm BS}^{\rm max} \\ d_{\rm RL}^{\rm max}$	Max. BS reach	900 m
$d_{\rm RL}^{\rm max}$	Max. relay hop	500 m
$d_{\mathrm{CH}}^{\mathrm{max}}$	CH-client radius	50 m
	Radio	
$\overline{P_t}$	UE/BS transmit power	23 dBm
$B_{UE-VBS}$	Per-link bandwidth	1 kHz
$R_{\min}$	Service-rate threshold	300 kbps
Trials	Iterations per $\lambda$	20
	AWGN-FSPL engine	
Path-loss exponent		2 (free space)
Shadowing $\sigma_{\text{shad}}$		$0\mathrm{dB}$
Interference		muted (SINR = SNR)
	LOGD engine	
Path-loss exponent $\alpha$		3.7 (urban NLOS)
Shadowing $\sigma_{\rm shad}$		6 dB
Interference		active (all links)
$\overline{f_c}$	Carrier frequency	3.5 GHz
$N_0$	Noise PSD	$-174\mathrm{dBmHz^{-1}}$

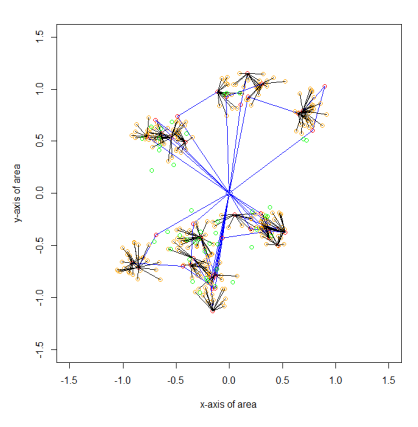
All radios—gNodeB, relay and cluster head—transmit  $P_t = 23 \, \text{dBm}$  on a 1 kHz resource block. The application floor is fixed at  $R_{\text{min}} = 300 \, \text{kbps}$ , which maps (via Eq. (6)) to the minimum admissible SINR. For every  $\lambda$  value the generator/solver chain executes 20 *iterations* and ensemble averages are reported.

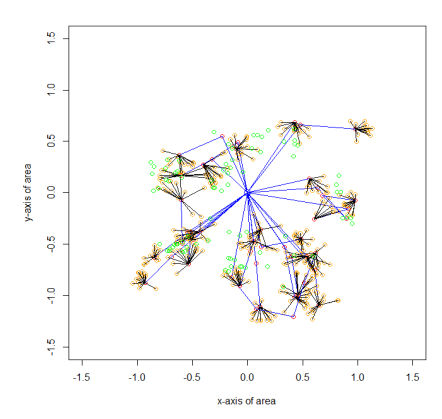
Propagation is examined under two regimes. (i) AWGN–FSPL: the path-loss exponent is fixed at 2, log-normal shadowing is disabled, and cross-link interference is muted, so the received SINR degenerates to the plain SNR. (ii) LOGD: an urban NLOS exponent  $\alpha=3.7$  is adopted, log-normal shadowing with standard deviation  $\sigma_{\rm shad}=6\,{\rm dB}$  is injected and the power of *all* simultaneous transmissions is accumulated as interference. Both regimes share a carrier frequency  $f_c=3.5\,{\rm GHz}$  and a thermal-noise density of  $N_0=-174\,{\rm dBm\,Hz^{-1}}$ . After every iteration each link's SINR is benchmarked against the threshold dictated by Eq. (6) to declare outages; the very same SINR traces drive Eqs. (10)–(13) to yield the spectral- and energy-efficiency curves discussed in Sections V-B–V-C.

All outage curves reported in Section VII-A were obtained by averaging over 20 independent simulation runs for each PPP intensity  $\lambda$ , i.e., each data point is the arithmetic mean of 20 separate network realizations. For the spectral-and energy-efficiency plots in Section VII-B, we performed 150 independent simulation runs per  $\lambda$  to ensure statistical smoothness.









(a) Max. hop allowed = 1,  $\lambda = 3$ 

(b) Max. hop allowed = 3,  $\lambda = 2$ 

(c) Max. hop allowed = 5,  $\lambda = 4$ 

FIGURE 7. Examples of varying generated topologies for UE-VBS computing networks/infrastructures. (Min. and Max. number of devices in a cluster is 8 to 14.).

#### A. OUTAGE NUMERICAL MODEL AND ASSUMPTIONS

To calculate the actual outage probability in our networks, we have to modify our path loss model and make several assumptions. Firstly, the simplistic path loss model used for our analysis is replaced with the empirical LOGD path loss model [33], [34]; the model supports Non-Line-of-Sight (NLOS) urban environments [30], [35], [36] with an assumed carrier frequency of 10KHz (rather than the usual 3.5 GHz (as in n78 band of 5G spectrum) [37]) with the purpose to show the improvements of our approach. Moreover, in the examination of the LOGD path loss model, the analytical and numerical examinations took place using the same path loss model. The LOGD path loss model's analytical and numerical results align, showing our concept's proof. It should be noted that we examine all models within the simulations. Secondly, the final outage probability is calculated by assuming that  $\{X\%\}$  of devices that are deemed to have a lower SINR than the threshold SINR<sub>TH</sub> will reflect the outage probability. We reinforce this measurement by repeating each calculation multiple times (around 20) and using the average as the final result.

A final assumption is that all of the transmitters, including the gNodeB BS, have the same transmitting power, which is unity in our case. This assumption is made to make analysis and simulation simple and manageable. Furthermore, this assumption is expected not to significantly impact the results because, in the case of the above two intensities, the number of transmitting devices is considerably large (20-150 times), which would make the interference effect of the initial BS has less impact. Fig. 8 and 9 (for LOGD) illustrate the general model used for our analysis. Our model operates in four main stages:

- 1) In the first stage, we decide on the parameters that will be used for the randomly generated network. These parameters include the following:
  - Size of the square area in which devices are generated.

- Intensity of parent points in the process, denoted as Φ.
- Standard deviation of secondary/child points in all clusters C.
- Average number of client points (UE devices).
- Percentage of randomly sampled devices that will become  $U_{UE-VBS}$ .
- Maximum number of UE-VBS hops allowed.
- Maximum range of the gNodeB BS.
- Maximum and minimum number of devices allowed in a cluster.
- Maximum and minimum range of devices in  $U_{AV-RL}$ .
- Maximum range of devices in  $U_{UE-VBS_{CH}}$ .
- 2) In the second stage, after defining these parameters, we generate the network accordingly.
- 3) In the third stage, we analyze the generated network based on the performance metrics we aim to obtain. These performance metrics are illustrated in Fig. 8 and Fig. 9 (for LOGD) and are discussed in the following paragraphs.
- 4) In the fourth stage, we provide a detailed description of the performance metrics and their implications.

#### **B. EFFICIENCY NUMERICAL MODELS AND ASSUMPTIONS**

The efficiencies are obtained using a similar workflow method as shown in Fig. 8, except that we now use the analytical expressions formulated in Section III to get spectral and energy efficiency results for the randomly generated power signals.

The only significant difference in the calculations is that the SINR that is received from the generated networks is either used to carry out the calculation shown in Eq. (13) for the spectral efficiency, or Eq. (14) for the energy efficiency. Also, we ran the simulation multiple times (150-200 times) to obtain a close value to the average between all results per intensity step.



Regarding the energy efficiency, we had some ambiguity with the values used for  $\beta-$  transmitted power ratio and  $\gamma-$  total data rate ratio. These values are used to calculate the total power our networks use (as shown in Eq. (15)), affecting energy efficiency. These values are crucial in making the result look like our earlier analysis, which is carried out by varying the number of devices to affect the data rate. To determine the optimum values for  $\beta$  and  $\gamma$ , after conducting a brute-force analysis, we found that the values 175 and  $3 \times 10^{-5}$  for  $\beta$  and  $\gamma$ , respectively, have yielded a satisfactory result.

#### **VII. PERFORMANCE EVALUATION AND RESULTS**

After going through the process described in Fig. 8 for randomly generated networks per intensity step, which was set to 0.5, we arrived at the results seen in Fig. 9 and 10. These figures show the numerical results (lines with dots) compared to the analytical solution.

#### A. OUTAGE PROBABILITY

This section examines the LOGD path loss model, comparing numerical results against analytical (FSPL model) predictions regarding outage probability in a telecommunications network.

# 1) EXAMINATION OF THE LOGD PATH LOSS MODEL IN TERMS OF OUTAGE PROBABILITY

By analyzing Fig. 9, we observe that the numerical results exhibit a consistent trend with the analytical predictions when examining the gradual increase in outage probability. The LOGD path loss model's trend does not exhibit a strictly linear increase or follow a negative exponential decay-like pattern. Rather, the numerical outage probability tends to level off, not reaching one even as PPP intensity ( $\lambda$ ) increases beyond 3, contrasting with the analytical expectations. The LOGD path loss model, which considers environmental factors and the logarithmic attenuation of signal strength over distance, results in a less aggressive growth of outage probability. This slower rate of increase suggests a model where signals may degrade less rapidly than predicted by the analytical model, which could be due to a less severe path loss or interference signals also experiencing attenuation, thereby having a smaller impact on the outage. Moreover, upon inspection of Fig. 9, we observe that the numerical results align closely with the analytical expectations up to a PPP intensity ( $\lambda$ ) of approximately 3, beyond which the numerical model diverges, flattening out and not reaching an outage probability of 1. This deviation suggests that the LOGD path loss model, which incorporates environmental factors and logarithmic signal attenuation over distance, yields a less pronounced growth in outage probability than the analytical model. This can indicate signals experiencing less degradation or interference signals being attenuated more than anticipated, hence having a less impactful effect on outage probability.

The mean cross-correlation with zero lag between the numerical and analytical results remains high, reflecting the relative similarity between the two approaches. Although initial results do not align perfectly with our analytical predictions, the mean cross-correlation for the LOGD path loss model is approximately 97.4%. It's important to note that while this suggests a high degree of alignment, crosscorrelation is sensitive to how it is calculated and primarily serves as a comparative metric within this study. However, the numerical outage only partially follows our analysis at higher intensities. The increase in outage begins to slow down and plateaus around 80% outage probability. The future analysis must integrate interference variability, potentially incorporating models that account for random distributions such as Rayleigh fading in the channels from the gNodeB to the first UE-VBS device.

The numerical and analytical results show a steeper initial rise in outage probability, followed by a plateau, leading to a lower overall outage in the numerical simulation. This suggests that the *SINR*<sub>TH</sub>, defined as an upper bound as in Eq. eq:6, is more relaxed in the numerical model, which could be attributed to the dampening effect of the LOGD path loss on interfering signals. Moreover, this trend implies that the *SINR*<sub>TH</sub>, established as an upper boundary in Eq. (6), may be more relaxed in the numerical and analytical model, a reflection of the LOGD path loss model's mitigation of interference.

Noteworthy, the zero-hop model, representing a direct connection between the base station (BS) and devices, shows improved alignment with analytical predictions after adjustments, indicating an initial spike in outage probability that then decreases. Conversely, multi-hop topologies—such as those with 1-hop, 2-hop, and 3-hop configurations demonstrate better initial network stability and reliability. This suggests that increasing hops can reduce strain on the BS, distribute network traffic more effectively, and decrease the risk of service disruptions. Multi-hop systems are particularly advantageous in dense urban environments where high demand and the need for consistent connectivity are critical. Although simpler and less costly, zero-hop systems could be enhanced by increasing BS capacity or employing advanced signal processing techniques. Implementing multi-hop networks can also contribute to overall network resilience and redundancy, safeguarding against widespread failure in case of localized issues, thus endorsing the benefits of adding hops within a network. Additionally, the assumption in the analytical model that each connection tree has numerous intermediate connections contrasts with the numerical model's limitation on the maximum number of connections. This distinction could explain the numerical model's lower observed outages at higher PPP intensities.

In summary, by tuning the parameters of the LOGD path loss model to reflect the real-world signal propagation and environmental factors more accurately, the numerical results become more sensitive to the proliferation of devices within the network. This results in a more harmonious



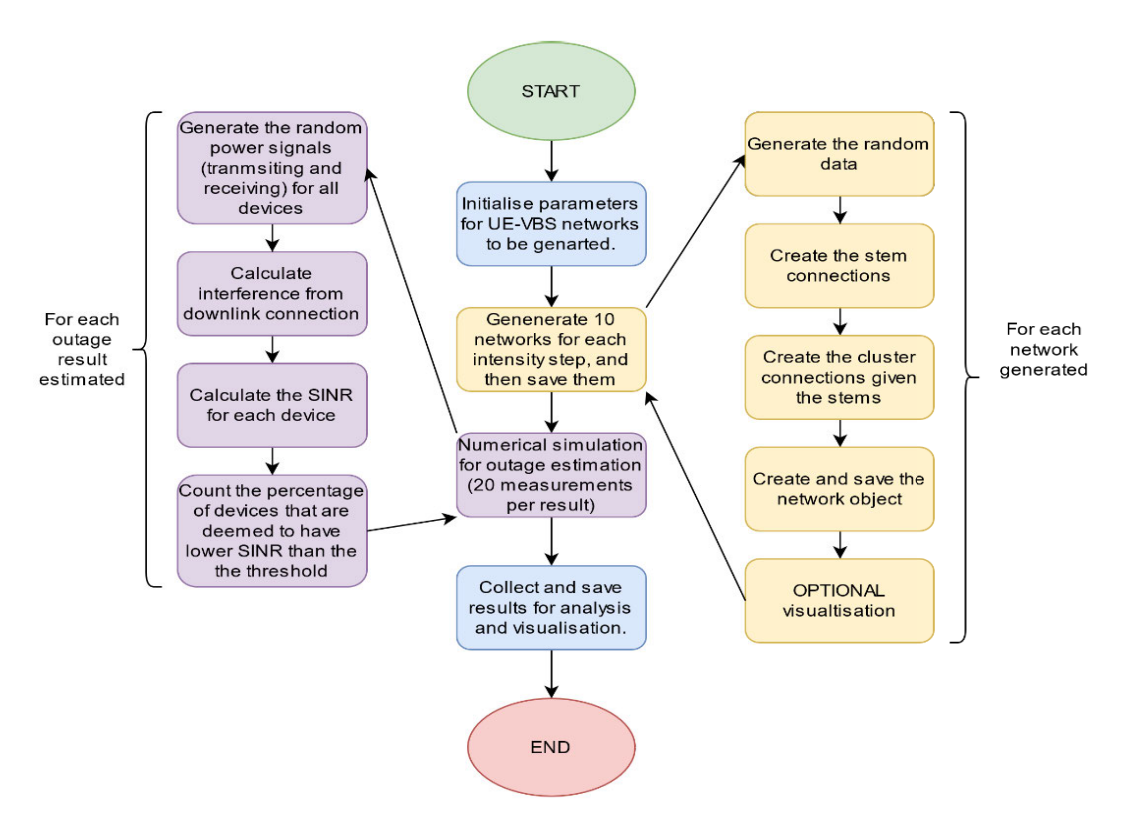
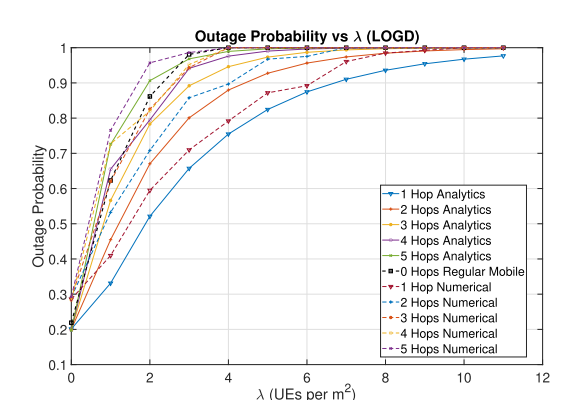


FIGURE 8. Computational simulation model workflow.



**FIGURE 9.** Comparison of outage probabilities using the LOGD path loss model for both numerical (solid lines) and analytical (dashed lines) approaches, underscoring the divergence in predictions for  $\lambda$  values beyond approximately 3..

performance with our analytical expectations, providing a refined perspective on network behavior under different conditions of device density and path loss.

# 2) CORRELATION BETWEEN FSPL (ANALYTICAL) AND LOGD (NUMERICAL) PATH LOSS MODEL RESULTS IN TERMS OF OUTAGE PROBABILITY

This section presents a correlation analysis between the LOGD path loss model (numerical) and the FSPL model (analytical), particularly in terms of outage probability as the

Poisson Point Process intensity ( $\lambda$ ) increases. Both models predict how signal attenuation and interference affect the probability of an outage in dense wireless networks. The numerical results from the LOGD model are compared to the analytical results derived from the FSPL model to assess their alignment under different network conditions. The LOGD path loss model, as shown in Fig. 9, aligns closely with analytical expectations at lower PPP intensities. This suggests that the LOGD model's consideration of environmental factors, such as signal attenuation and interference from obstacles, is effective in environments with lower device density. However, as the PPP intensity increases, the LOGD model outage probability tends to level off, indicating that interference and environmental effects become less significant beyond a certain point. This plateau effect demonstrates how the LOGD model accounts for real-world factors, limiting the rise in outage probability as environmental attenuation reduces the overall impact of interference.

On the other hand, the FSPL model predicts a more aggressive increase in outage probability at higher PPP intensities, as it assumes ideal free-space propagation without accounting for environmental obstructions. In this model, interference increases with device density, causing a steady rise in the outage probability, eventually approaching unity. The FSPL model's analytical predictions are useful in understanding ideal scenarios, but they lack the realism introduced by the environmental considerations of the LOGD model. The



correlation between the LOGD model's numerical results and the FSPL model's analytical results is high, with cross-correlation values of approximately 93%, and 97.4%, respectively. This high degree of similarity underscores the effectiveness of the LOGD model in capturing the general trend of outage probability increasing with PPP intensity while also reflecting the real-world effects of environmental factors, which are absent in the FSPL model. In multihop configurations, the LOGD model demonstrates superior performance, as it accounts for signal attenuation and the impact of intermediate nodes on improving network stability. In contrast, the FSPL model, which does not factor in environmental attenuation, is less effective at predicting the benefits of multi-hop scenarios, particularly in dense environments where interference plays a significant role. As a result, the LOGD model is better suited for modeling realistic urban or densely populated scenarios where obstacles and environmental factors affect signal propagation.

In conclusion, while the FSPL model provides a valuable analytical baseline, particularly in ideal free-space environments, the LOGD path loss model offers a more accurate representation of network behavior in real-world conditions. The LOGD model's ability to incorporate environmental impacts, such as signal attenuation due to obstacles, makes it a more reliable choice for predicting outage probability in urban or dense environments where signal degradation and interference significantly influence network performance. Future work should focus on refining these models to further improve the correlation between numerical and analytical results, particularly by enhancing the realism of the FSPL model in non-ideal environments.

# 3) ZERO-HOP (REGULAR MOBILE) VERSUS MULTI-HOP NETWORK PERFORMANCE

The performance improvements introduced by the UE-VBS in multi-hop scenarios are evident when comparing zero-hop direct connections to multi-hop configurations. In the LOGD path loss model shown in Fig. 9, multi-hop configurations with UE-VBS exhibit a more stable and gradual increase in outage probability, in contrast to the zero-hop scenario, where a steeper rise in outage probability is observed initially. This underscores the effectiveness of UE-VBS in maintaining network performance even as PPP intensity escalates.

The comparison across different hop scenarios demonstrates that the LOGD path loss model benefits significantly from deploying UE-VBS. Multi-hop networks with UE-VBS are more robust against signal degradation, particularly in dense network environments, which is consistent with the lower outage probabilities observed in the numerical results. These findings reinforce the potential of UE-VBS to enhance network performance, offering a compelling case for its integration into modern telecommunication systems. Therefore, future network design considerations should include the strategic placement of UE-VBS to optimize coverage and reliability, particularly in areas with

high user density and diverse environmental conditions. The advantages of multi-hop configurations over zero-hop setups, as demonstrated in the comparative analysis, highlight their efficacy in enhancing the robustness and efficiency of telecommunications networks.

#### **B. EFFICIENCIES**

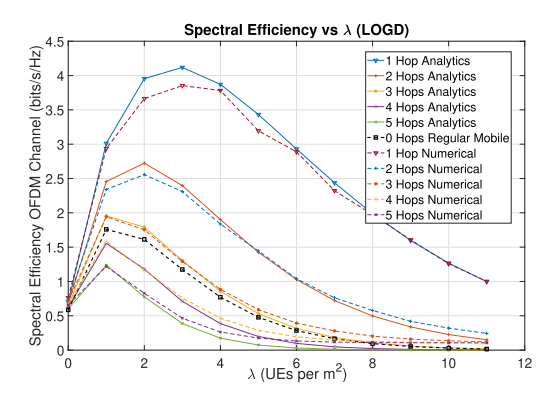
This section examines spectral and power efficiency regarding the LOGD path loss model, comparing numerical results against analytical (FSPL Model) predictions. Additionally, it provides a comparative analysis where the spectral and energy efficiencies under different hop strategies were analyzed. Furthermore, the performance implications of the observed cross-correlation factors have been discussed.

# 1) EXAMINATION OF THE LOGD PATH LOSS MODEL IN TERMS OF EFFICIENCIES

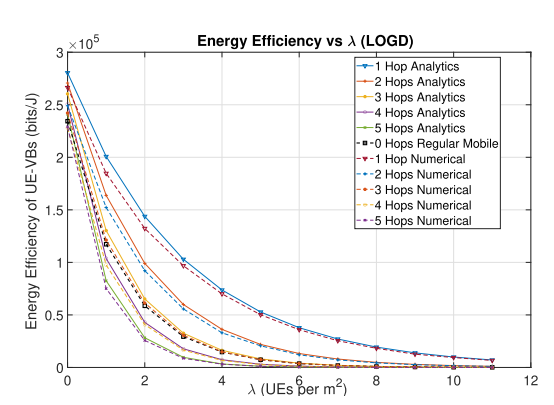
This section examines spectral and power efficiency regarding the LOGD path loss model. Additionally, it provides a comparative analysis where the spectral and energy efficiencies under different hop strategies were analyzed. Furthermore, the performance implications based on the observed cross-correlation factors have been discussed. Through meticulous analysis of the LOGD path loss model, our finalized results, delineated in Fig. 10, are set in comparison with the analytical model. We observed exceptionally high cross-correlation values of 99.83% for Spectral efficiency and 99.9% for Energy efficiency. These figures indicate an exceptionally precise congruence with our controlled simulation parameters, as described in Sections V-B and V-C, respectively.

analyzing the spectral efficiency visualised in Fig. 10, we note an overarching concordance with the analytical model, punctuated by marginal deviations. The most notable observation is the distinct ascendancy of a one-hop (n = 1) topology over the multi-hop configurations, plausibly attributed to a lessened concentration of adversarial transmitters. The multi-hop frameworks  $(n \neq 1)$  demonstrate a levelled performance range, insinuating a potential uniformity in interference and signal patterns, thereby normalizing SINR. The numerical perturbations render the peak, which is prominent in the analytical findings, less discernible, signalling a need for further refinement to sharpen spectral efficiency optimization. In contrast to the analytic projections, numerical data does not exhibit a decline towards zero as PPP intensity escalates, which suggests an area for further scrutiny. Turning to energy efficiency as portrayed in Fig. 10b, the numerical results manifest a near-perfect mirroring of the analytical benchmarks. This parallelism likely emanates from the precise emulation of hardwarespecific determinants, including data rate and transmission power ratios. Despite the numerical noise, the preeminent trend of exponential decay is retained, underscoring the empirical soundness of the LOGD path loss model.





(a) Numerical and Analytical Results for Spectral Efficiency utilizing the LOGD path loss model, achieving a cross-correlation of 99.83%.



(b) Numerical and Analytical Results for Energy Efficiency employing the LOGD path loss model, with a cross-correlation of 99.9%.

FIGURE 10. Numerical analysis juxtaposed with analytical computations elucidating the efficiency metrics of the UE-VBS framework governed by the LOGD path loss model..

Spectral Efficiency: The LOGD path loss model demonstrates that multi-hop approaches, especially the one-hop scenario, show superior spectral efficiency over the zero-hop configuration.

Energy Efficiency: The energy efficiency graph for the LOGD path loss model corroborates the superiority of multi-hop strategies over zero-hop. One-hop remains the most energy-efficient across varying PPP intensities.

# 2) CORRELATION BETWEEN FSPL (ANALYTICAL) AND LOGD (NUMERICAL) PATH LOSS MODEL RESULTS IN TERMS OF

This subsection provides an analysis of the correlation between the FSPL path loss model (analytical) and the LOGD path loss model (numerical). The analysis focuses on how closely the numerical results obtained from the LOGD path loss model align with the analytical predictions based on the FSPL model. The models were evaluated for both spectral and energy efficiency.

#### a: SPECTRAL EFFICIENCY CORRELATION

In the FSPL path loss model (analytical), the spectral efficiency predictions provided a baseline for comparison with the numerical results of the LOGD model. The numerical simulations of the LOGD model achieved a cross-correlation factor of 99.83% with the analytical FSPL predictions (see Fig. 10). This high correlation indicates that the LOGD model effectively captures the spectral efficiency trends predicted by the FSPL model, particularly at lower PPP intensities. However, the LOGD model better accommodates real-world factors such as environmental attenuation, maintaining consistent spectral efficiency even at higher PPP intensities, which the FSPL model, assuming ideal conditions, does not fully account for.

Spectral efficiency trends observed in the LOGD model were:

$$\eta_{spectral}(n) = \begin{cases} \text{Stable or slight decrease} \\ \text{for } n = 0 \text{ (Zero-Hop Mobile)} \end{cases}$$

$$\text{Peak at lower PPP intensity}$$

$$\text{for } n = 1 \text{ (Single-Hop)}$$

$$\text{Convergent performance}$$

$$\text{for } n > 1 \text{ (Multi-Hop)}$$

#### b: ENERGY EFFICIENCY CORRELATION

The energy efficiency results from the LOGD model (numerical) achieved a cross-correlation of 99.9% with the FSPL model (analytical), as shown in Fig. 10b. The FSPL model served as the analytical baseline, and the high correlation suggests that the LOGD model accurately simulates the energy efficiency trends predicted analytically by FSPL, particularly in multi-hop configurations. The LOGD model, however, includes environmental factors such as shadowing and interference, which contribute to its higher accuracy in real-world scenarios compared to the idealised FSPL model.

Energy efficiency trends observed in the LOGD model were:

$$\eta_{energy}(n) = \begin{cases} \text{Higher efficiency at lower PPP} \\ \text{for } n = 0 \text{ (Zero-Hop Mobile)} \\ \text{Exponential decay trend} \\ \text{for } n \ge 1 \text{ (Multi-Hop)} \end{cases}$$

#### c: SUMMARY

The high correlation factors between the LOGD (numerical) and FSPL (analytical) models demonstrate that the LOGD model is a reliable representation of real-world performance. While the FSPL model provides a strong analytical baseline, the LOGD model's inclusion of real-world factors like



TABLE 4. LOGD Path Loss Model Efficiency Comparison.

Configuration	Spectral Efficiency	Energy Efficiency
Zero-Hop	Lowest	Lowest
One-Hop	Highest peak	More efficient
Two-Hop	Lower than One-Hop	Comparable to One-Hop
Three-Hop	Lower than One-Hop	Less efficient than One-Hop
Four-Hop	Lower than One-Hop	Less efficient than One-Hop
Five-Hop	Lowest among multi-hop	Lowest among multi-hop

interference and environmental attenuation makes it more suitable for practical network designs. Future work could focus on refining the LOGD model further to enhance its predictive accuracy across varying environmental and network conditions.

# 3) COMPARISON OF ZERO-HOP MOBILE APPROACH AND MULTI-HOP CONFIGURATIONS USING LOGD PATH LOSS MODEL

The performance of zero-hop and multi-hop network configurations using the LOGD path loss models was thoroughly analyzed to determine their impact on the system efficiency and outage probability. This section details the comparative results of these configurations. Using the LOGD path loss model, the zero-hop configuration exhibits the lowest efficiency in both spectral and energy terms, significantly under-performing compared to other setups. In contrast, the one-hop configuration demonstrated superior performance, maintaining a clear advantage in terms of lower outage probability and higher efficiency. This is largely attributed to avoiding the compounding effects of path loss over multiple hops (see Fig. 9). According to Table 4, the one-hop setup achieves the highest peak in spectral efficiency and is also more energy-efficient. Multi-hop configurations, though slightly better aligned with analytical predictions, still experience a decline in performance with each additional hop. Specifically, configurations with two to five hops show progressively lower spectral and energy efficiencies, with five-hop configurations displaying the lowest efficiency among the multi-hop setups.

#### a: LOG PATH LOSS MODEL

Similar trends were observed in the LOGD path loss model, where the zero-hop configuration exhibits the lowest efficiency in both spectral and energy terms, significantly underperforming compared to other setups. In contrast, the one-hop configuration demonstrated superior performance, maintaining a clear advantage in terms of lower outage probability and higher efficiency. This is largely attributed to avoiding the compounding effects of path loss over multiple hops (see Fig. 9). According to Table 4, the one-hop setup achieves the highest peak in spectral efficiency and is also more energy-efficient. Multi-hop configurations, though slightly better aligned with analytical predictions, still experience a decline in performance with each additional hop. Specifically, configurations with two to five hops show progressively lower spectral and energy efficiencies,

**TABLE 5.** Performance Analysis of Zero-Hop Mobile vs. Multi-Hop Approaches.

Hop Strategy	Spectral Efficiency	Energy Efficiency
Zero-Hop Mobile Single-Hop Multi-Hop	Baseline stability Best peak performance Convergent at high PPP	High efficiency at low PPP Good balance Decreases with PPP

with five-hop configurations displaying the lowest efficiency among the multi-hop setups.

#### b: SUMMARY

The LOGD path loss model confirms that the zero-hop configuration (the mobile regular case Base station with UEs) is the least effective in terms of spectral and energy efficiencies. These findings contrast sharply with the onehop configurations, which are generally more effective than multi-hop ones due to their simpler transmission paths and reduced exposure to interference. Table 4 underscores that while the one-hop setup achieves the highest peaks in both spectral and energy efficiencies, multi-hop configurations, although they extend the coverage, introduce increased path loss and interference. These added complexities can significantly diminish the network's overall performance, especially as the number of hops increases. In future network designs and optimizations, particularly in dense urban environments, these trade-offs should be carefully considered. The choice between zero-hop, one-hop, and multi-hop configurations could profoundly impact the quality of service and system robustness.

#### **VIII. CONCLUSION AND FUTURE WORK**

Our investigation into the feasibility and design of the UE-VBS computing paradigm has provided us with an analytical framework for calculating the outage probability of a general network. It has also initialised the optimization problem of such networks through network efficiencies. The efficacy of our analysis has been partially backed by numerical simulation, which we created firsthand in R due to the novelty of such a communication paradigm. Our simulation showed a cross-correlation measurement with the analysis, between 66.9% for spectral efficiency and 97% for our energy efficiency. Our study relies on certain justified assumptions discussed in Section II. However, the analysis does not account for OFDMA modulation of wireless signals. We are potentially missing the effect that multiple subcarriers would have on each other and the final outage result. These assumptions do take a certain, but presumably small, toll on our final results but allow for a simple and methodical approach to outage and wireless network performance prediction.

Note that we employed a simplified channel model in the theoretical analysis to provide a clear and digestible exposition of the core principles underpinning the UE-VBS computing system. For the simulations, a more comprehensive and realistic channel model was utilised to mirror



actual network conditions more closely, thereby ensuring the robustness and practical applicability of our theoretical findings. This strategy not only clarifies the foundational aspects of our proposal but also validates its effectiveness and efficiency through empirical simulations, effectively bridging the gap between theory and practical implementation. In our investigation, we utilized the LOGD path loss model to assess the efficiencies and outage probabilities of UE-VBS computing systems under varied operational conditions. Our comparative analysis revealed nuanced insights into the model's performance. For outage probabilities, the LOGD path loss model, while aligning with analytical expectations at lower intensities, levels off at higher  $\lambda$  values (see Fig. 9). The model shows a high mean cross-correlation value, approximately 97.4%, indicating its capability to track the increasing trend of outage probability accurately. However, the observed plateau at higher intensities highlights the need for model refinement to address complex interactions such as interference and environmental factors.

Additionally, the LOGD path loss model demonstrates superior reliability and alignment with analytical benchmarks in terms of system design and optimization, making it more suitable for applications requiring high precision in performance predictions. Both models provide valuable insights, yet future enhancements should focus on improving numerical simulations to minimize noise and align more closely with analytical predictions. This approach will enable more effective optimization of network configurations, incorporating stochastic elements like Rayleigh fading to better address observed discrepancies. In our analysis of the zero-hop configuration across different path loss models—specifically the LOGD path loss models we observed distinct performance challenges. The zero-hop configuration, characterized by direct connections between user equipment and the base station, consistently demonstrated higher outage probabilities, particularly at initial point-to-point protocol (PPP) intensities. This indicates a vulnerability in network resilience and coverage without the intermediation of multi-hop setups involving UE-VBSs. Furthermore, in terms of spectral and energy efficiencies, the zero-hop configuration emerged as the least effective. This inefficiency can be attributed to its simpler, yet more exposed transmission paths, which do not benefit from the relay and amplification advantages present in multi-hop scenarios. Consequently, while zero-hop configurations may offer straightforward connectivity, they lack the robustness required for optimal performance in dense and dynamically changing network environments. These insights suggest that despite the operational simplicity of zero-hop configurations, their use in future network designs should be carefully evaluated, particularly in scenarios where high system robustness and low outage probabilities are critical. The comparative inefficiency in both spectral and energy terms underscores the potential benefits of integrating more complex multi-hop configurations, especially in dense urban settings. Also, we will quantify how the UE-VBS framework scales as the UE density  $\lambda$  and VBS-capable fraction u increase. Specifically, we plan to measure outage probability, spectral/energy efficiency and control-plane signaling overhead under both a centralized controller (all clustering decisions at the gNodeB) and a fully distributed scheme (local UE elections via our decision-tree rule). This will expose the signaling vs. performance trade-off inherent in virtualized architectures operating at extreme densification. We will also investigate UE-centric scheduling (resource grants tailored per-UE based on local CQI and battery state) [38], resource virtualization (abstraction of physical air-interface and compute resources into shareable virtual pools) [39], and network slicing (partitioning of a common infrastructure into isolated end-to-end service instances with SLAs and orchestration via 5G-core APIs) [40]. This will expose the signaling vs. performance trade-off inherent in virtualized architectures operating at extreme densification. From a sustainability perspective, the proposed UE-VBS and cellfree communication architecture promotes greener and more energy-efficient wireless networks by reducing dependence on centralized infrastructure and enhancing local processing capabilities. By minimizing backhaul usage and improving spectral and energy efficiency, this approach contributes to the design of low-carbon and sustainable 6G networks. Such developments are aligned with the broader goals of green communications and sustainable digital infrastructures as emphasized in recent literature [41], [42], and support the United Nations' Sustainable Development Goals (SDGs), particularly those related to affordable and clean energy and industry innovation.

Future work will focus on refining the outage analysis and efficiency models by reducing assumptions, enhancing the numerical simulations, and incorporating more realistic system parameters. We will also explore hardware implementations to optimize the system for practical deployment. Moreover, recognizing the importance of real-world validations, we plan to explore and incorporate practical implementations and experimental results in future work. This will involve developing test-beds to demonstrate the UE-VBS configurations' practical feasibility and real-world performance under varied environmental conditions. Such efforts will validate the theoretical predictions and provide insights into practical challenges and optimizations necessary for deployment.

In addition, we intend to replace the baseline random-sampling rule (fixed u) with a metric-driven selection scheme by computing for each UE a suitability score  $S_i = w_b \, b_i + w_s \, \frac{\text{SINR}_i}{\text{SINR}_{\text{max}}} + w_d \, \left(1 - \frac{d_i}{d_{\text{max}}}\right) + w_c \, \frac{c_i}{c_{\text{max}}}$  and promoting the highest-scoring devices to UE-VBS cluster heads. We will also investigate adaptive strategies in which u varies dynamically with network load or UE density, potentially managed via feedback loops or reinforcement-learning agents. Furthermore, we plan to develop supervised machine-learning classifiers—such as decision trees or random forests—trained on real UE telemetry (battery level, link quality, processing load) to predict the best cluster-head



candidates. Extensions to support UE mobility, handover between clusters, and the cost of re-electing heads in dynamic environments will be explored. Finally, we aim to implement a small-scale prototype testbed using commodity smartphones or software-defined radios to measure outage probability, throughput and energy consumption under real operating conditions, thus closing the gap between theory and practice. We will extend our future work to rigorously quantify the battery impact of UE-VBS relays by integrating detailed per-UE power consumption models into our simulation framework. This will include differentiating between normal uplink/downlink operation and relay/clusterhead duties (RF transmit, receive and baseband processing energy costs), measuring the incremental energy per relay hop under realistic traffic and mobility patterns, and evaluating power-management strategies such as duty-cycling and sleep modes to mitigate any extra drain. To ground these models in practice, we will also conduct small-scale experiments on commodity smartphones or SDR platforms to directly measure battery-drain during relay operation, and explore incentive mechanisms (e.g., data credits or reduced service fees) to fairly compensate users who volunteer as UE-VBS nodes.

Additionally, in our future work, we will investigate the impact of non-ideal hardware components—such as finite-resolution phase shifters, power amplifier nonlinearities, and oscillator phase noise—which introduce residual distortion and impose a performance ceiling in practical wireless systems, particularly in the high-SNR regime. For example, active RIS-aided links suffer from phase-shift noise and imperfect CSI that limit array gains at elevated transmit powers. In STAR-RIS-assisted NOMA uplinks, hardware impairments combined with channel estimation errors degrade the achievable sum-rate even at high SNRs. Similarly, reconfigurable holographic surfaces in near-field cell-free networks exhibit significant performance loss when RF-chain imperfections are accounted for, and energy-efficient holographic metasurfaces must balance realistic impairment models against power consumption to avoid throughput collapse at high SNR. In the UE-VBS paradigm, commodity UEs acting as relays and cluster heads face the same transceiver imperfections; at high D2D transmit powers, finite DAC/ADC resolution, PA non-linearities, and oscillator phase noise induce residual distortion that caps end-to-end SINR and data rates. To capture these effects, we will incorporate a per-hop additive "impairment noise" term—analogous to those used in RIS studies—directly into each UE-VBS link's SINR expression, ensuring our outage and spectral/energy-efficiency analyses reflect the true performance ceiling of real-world deployments under strongsignal conditions [43], [44], [45], [46].

#### **REFERENCES**

 C. Christophorou, A. Pitsillides, and I. Akyildiz, "CelEc framework for reconfigurable small cells as part of 5G ultra-dense networks," in *Proc. IEEE Int. Conf. Commun. (ICC)*, May 2017, pp. 1–7.

- [2] I. Ioannou, P. Nagaradjane, C. Christophorou, V. Vassiliou, G. V. S. Sashank, C. Jain, and A. Pitsillides, "ML-aided dynamic clustering and classification of ues as vbs in D2D communication networks," in *Proc. Int. Conf. Wireless Commun. Signal Process. Netw. (WiSPNET)*, 2023, pp. 1–8.
- [3] K. Venkateswararao, P. Swain, C. Christophorou, and A. Pitsillides, "Using UE-VBS for dynamic virtual small cells deployment and backhauling in 5G ultra-dense networks," *Comput. Netw.*, vol. 189, Apr. 2021, Art. no. 107926.
- [4] R. Ahmad, E. A. Sundararajan, and A. Khalifeh, "A survey on femtocell handover management in dense heterogeneous 5G networks," *Telecommun. Syst.*, vol. 75, no. 4, pp. 481–507, Dec. 2020.
- [5] I. Ioannou, V. Vassiliou, C. Christophorou, and A. Pitsillides, "Distributed artificial intelligence solution for D2D communication in 5G networks," *IEEE Syst. J.*, vol. 14, no. 3, pp. 4232–4241, Sep. 2020.
- [6] M. Haenggi, Stochastic Geometry for Wireless Networks. Cambridge, U.K.: Cambridge Univ. Press, 2013.
- [7] J. G. Andrews, R. K. Ganti, M. Haenggi, N. Jindal, and S. Weber, "A primer on spatial modeling and analysis in wireless networks," *IEEE Commun. Mag.*, vol. 48, no. 11, pp. 156–163, Nov. 2010.
- [8] M. Afshang, C. Saha, and H. S. Dhillon, "Nearest-neighbor and contact distance distributions for Thomas cluster process," *IEEE Wireless Commun. Lett.*, vol. 6, no. 1, pp. 130–133, Jan. 2016.
- [9] P. Swain, C. Christophorou, U. Bhattacharjee, C. M. Silva, and A. Pitsillides, "Selection of UE-based virtual small cell base stations using affinity propagation clustering," in *Proc. 14th Int. Wireless Commun. Mobile Comput. Conf. (IWCMC)*, Jun. 2018, pp. 1104–1109.
- [10] J. R. S. Veluswami, I. Ioannou, P. Nagaradjane, C. Christophorou, V. Vassiliou, D. Nivedhitha, M. Sriram, and A. Pitsillides, "A twostage machine learning approach for 5G mobile network augmentation through dynamic selection and activation of UE-VBSs," SSRN Electron. J., pp. 1–21, Jan. 2022.
- [11] K. Venkateswararao and P. Swain, "Dynamic selection of virtual small base station in 5G ultra-dense network using initializing matching connection algorithm," in *Proc. IEEE Int. Conf. Adv. Netw. Telecommun.* Syst. (ANTS), Mar. 2019, pp. 1–6.
- [12] L. Wang, R. Chai, H. Chen, and Q. Chen, "Joint mode selection, VBS association and resource allocation for cellular D2D communication networks," in *Proc. Int. Conf. Comput., Netw. Commun. (ICNC)*, Mar. 2018, pp. 800–804.
- [13] A. R. Danisya, G. Hendrantoro, and P. Handayani, "UE clustering based on grid affinity propagation for mmWave D2D in virtual small cells," in *Proc. IEEE Int. Conf. Ind. 4.0, Artif. Intell., Commun. Technol. (IAICT)*, Jul. 2023, pp. 38–44.
- [14] K. Venkateswararao, P. Swain, S. S. Jha, I. Ioannou, and A. Pitsillides, "A novel power consumption optimization framework in 5G heterogeneous networks," *Comput. Netw.*, vol. 220, Jan. 2023, Art. no. 109487.
- [15] K. Venkateswararao and P. Swain, "Binary-PSO-based energy-efficient small cell deployment in 5G ultra-dense network," J. Supercomput., vol. 78, no. 1, pp. 1071–1092, Jan. 2022.
- [16] B. J. Frey and D. Dueck, "Clustering by passing messages between data points," *Science*, vol. 315, no. 5814, pp. 972–976, Feb. 2007.
- [17] M. Duarte, C. Dick, and A. Sabharwal, "Experiment-driven characterization of full-duplex wireless systems," *IEEE Trans. Wireless Commun.*, vol. 11, no. 12, pp. 4296–4307, Dec. 2012.
- [18] H. Zhang et al., "Full-duplex wireless communications: Prototypes and experiments," *IEEE Commun. Mag.*, vol. 57, no. 12, pp. 136–142, Dec. 2019, doi: 10.1109/MCOM.2019.1800243.
- [19] M. Duarte and A. Sabharwal, "Full-duplex wireless communications using off-the-shelf radios: Feasibility and first results," in *Proc. 44th Asilomar Conf. Signals, Syst. Comput.*, Nov. 2010, pp. 1558–1562.
- [20] Z. Zhang, K. Long, A. V. Vasilakos, and L. Hanzo, "Full-duplex wireless communications: Challenges, solutions, and future research directions," *Proc. IEEE*, vol. 104, no. 7, pp. 1369–1409, Jul. 2016.
- [21] J. T. J. Penttinen, 5G Explained: Security and Deployment of Advanced Mobile Communications. Hoboken, NJ, USA: Wiley, Apr. 2019.
- [22] R. T. Tse, Wireless Communications: Principles and Practice. Upper Saddle River, NJ, USA: Prentice-Hall, 2001.
- [23] B. P. Lathi and Z. Din, Modern Digital and Analog Communication Systems. London, U.K.: Oxford Univ. Press, 2010.



- [24] LTE Direct Always-On Device-to-Device Proximal Discovery, 3rd Gener. Partnership Project (3GPP), Sophia Antipolis, France, 2014.
- [25] C. E. Shannon, "A mathematical theory of communication," Bell Syst. Tech. J., vol. 27, no. 3, pp. 379–423, Jul. 1945.
- [26] L. Zhang, H.-C. Yang, and M. O. Hasna, "Generalized area spectral efficiency: An effective performance metric for green wireless communications," *IEEE Trans. Commun.*, vol. 62, no. 2, pp. 747–757, Feb. 2014.
- [27] A. Goldsmith, Wireless Communications, document Ee359, 2020.
- [28] M. Abramowitz and I. A. Stegun, Handbook of Mathematical Functions With Formulas, Graphs, and Mathematical Tables, vol. 55. Washington, DC, USA: National Bureau of Standards Applied Mathematics Series, 1964.
- [29] J. Aráuz, P. Krishnamurthy, and M. A. Labrador, "Discrete Rayleigh fading channel modeling," Wireless Commun. Mobile Comput., vol. 4, no. 4, pp. 413–425, Jun. 2004.
- [30] S. Sun, T. S. Rappaport, S. Rangan, T. A. Thomas, A. Ghosh, I. Z. Kovacs, I. Rodriguez, O. Koymen, A. Partyka, and J. Jarvelainen, "Propagation path loss models for 5G urban micro- and macro-cellular scenarios," in *Proc. IEEE 83rd Veh. Technol. Conf. (VTC Spring)*, May 2016, pp. 1–6.
- [31] S. Ali, M. Zeeshan, and A. Naveed, "A capacity and minimum guarantee-based service class-oriented scheduler for LTE networks," EURASIP J. Wireless Commun. Netw., vol. 2013, no. 1, p. 67, Dec. 2013.
- [32] M. Afshang, H. S. Dhillon, and P. H. Joo Chong, "Modeling and performance analysis of clustered device-to-device networks," *IEEE Trans. Wireless Commun.*, vol. 15, no. 7, pp. 4957–4972, Jul. 2016.
- [33] F. Comeau, S. C. Sivakumar, W. J. Phillips, and W. Robertson, "A clustered wireless sensor network model based on log-distance path loss," in *Proc. 6th Annu. Commun. Netw. Services Res. Conf. (CNSR)*, May 2008, pp. 366–372.
- [34] A. Karttunen, C. Gustafson, A. F. Molisch, R. Wang, S. Hur, J. Zhang, and J. Park, "Path loss models with distance-dependent weighted fitting and estimation of censored path loss data," *IET Microw., Antennas Propag.*, vol. 10, no. 14, pp. 1467–1474, Nov. 2016.
- [35] J. Turkka and M. Renfors, "Path loss measurements for a non-line-of-sight mobile-to-mobile environment," in *Proc. 8th Int. Conf. ITS Telecommun.*, Oct. 2008, pp. 274–278.
- [36] L. Liao, R. J. Drost, Z. Li, T. Lang, B. M. Sadler, and G. Chen, "Long-distance non-line-of-sight ultraviolet communication channel analysis: Experimentation and modelling," *IET Optoelectron.*, vol. 9, no. 5, pp. 223–231, Oct. 2015.
- [37]  $\overline{5G}$  FR Bandwidth. Accessed: Feb. 1, 2025. [Online]. Available: https://www.sharetechnote.com/html/5G/5GFRBandwidth.html
- [38] Evolved Universal Terrestrial Radio Access (E-UTRA); Physical Channels and Modulation, document TS 36.211, 3GPP, 2020.
- [39] M. van der Ham, R. Otten, and A. Pras, "Network function virtualization: Challenges and applicability for wireless networks," *IEEE Commun. Mag.*, vol. 53, no. 2, pp. 90–97, Feb. 2015.
- [40] P. Rost, C. Mannweiler, D. S. Michalopoulos, C. Sartori, V. Sciancalepore, N. Sastry, O. Holland, S. Tayade, B. Han, D. Bega, D. Aziz, and H. Bakker, "Network slicing to enable scalability and flexibility in 5G mobile networks," *IEEE Commun. Mag.*, vol. 55, no. 5, pp. 72–79, May 2017.
- [41] M. Chiang and T. Zhang, "Sustainable 6G: A new era for green communications," *IEEE Internet Things J.*, vol. 10, no. 9, pp. 7181–7195, May 2023.
- [42] L. You, X. Huang, J. Choi, and D. Zhang, "Energy-efficient 6G for sustainable future: Enabling technologies, opportunities, and challenges," *IEEE Netw.*, vol. 35, no. 4, pp. 158–164, Apr. 2021.
- [43] Q. Li, M. El-Hajjar, I. A. Hemadeh, D. Jagyasi, A. Shojaeifard, and L. Hanzo, "Performance analysis of active RIS-aided systems in the face of imperfect CSI and phase shift noise," *IEEE Trans. Veh. Technol.*, vol. 72, no. 6, pp. 8140–8145, Jun. 2023.
- [44] Q. Li, M. El-Hajjar, Y. Sun, I. A. Hemadeh, A. Shojaeifard, Y. Liu, and L. Hanzo, "Achievable rate analysis of the STAR-RIS-aided NOMA uplink in the face of imperfect CSI and hardware impairments," *IEEE Trans. Commun.*, vol. 71, no. 10, pp. 6100–6114, Oct. 2023.
- [45] Q. Li, M. El-Hajjar, Y. Sun, and L. Hanzo, "Performance analysis of reconfigurable holographic surfaces in the near-field scenario of cell-free networks under hardware impairments," *IEEE Trans. Wireless Commun.*, vol. 23, no. 9, pp. 11972–11984, Sep. 2024.
- [46] Q. Li, M. El-Hajjar, Y. Sun, I. A. Hemadeh, A. Shojaeifard, and L. Hanzo, "Energy-efficient reconfigurable holographic surfaces operating in the presence of realistic hardware impairments," 2024, arXiv:2405. 01146



IACOVOS I. IOANNOU (Senior Member, IEEE) received the Associate degree in computer science from Cyprus College, in 2001, the B.Sc. degree in computer science from the University of Cyprus, in 2006, the M.Sc. degree (Hons.) in computer and network security from the Open University of Cyprus, in 2017, and the Ph.D. degree from the University of Cyprus, in 2021, focusing on telecommunications with AI/ML. He is currently a Researcher with the Networks Research Lab-

oratory, University of Cyprus. He is also a Junior Researcher with the Smart Networked Systems Research Group, RISE Center. His research interests include mobile and wireless communications, next-generation networks (5G), and device-to-device (D2D) communications using artificial intelligence techniques. He is a highly skilled developer with 20 years of hands-on working experience in the IT industry, ranging in the spectrum of IT systems from analysis, development, installation, and management. He was with the Phileleftheros Publishing Group as an IT Administrator and a Programmer for seven years, he was with Cyprus Stock Exchange as an IT and a Programmer for seven years. He worked at Primetel for six years as an IT and Software Engineer with the Services Department. He has vast experience with cellular network infrastructure and all modern development platforms and languages. He has a certificate in ICONIX/SCRUM. He is also a CCNET Certified from CISCO.



**ALA' KHALIFEH** received the Ph.D. degree in electrical and computer engineering from the University of California at Irvine, as a Fulbright Scholar.

He is currently an esteemed academic in the field of wireless sensor networks, IoT, and networking. He is also the Vice-Dean of the Deanship of Innovation, Technology Transfer, and Entrepreneurship (DI-TECH) and an Associate Professor with German Jordanian University

(GJU). Throughout his career, he has held pivotal roles in both academia and industry, including an Assistant Professor with German University in Cairo and leadership positions within IEEE, such as the Chair of the IEEE Jordan Section. His research contributions include over 115 Scopus-indexed publications. He has been awarded numerous prestigious accolades, such as the Leader of Innovation Fellowship (LIF) from the Royal Academy of Engineering (U.K.) and the Young AFCEA 40 under 40 International Award. Beyond academia, he has been instrumental in fostering collaboration between research institutions and industry, securing multiple research grants from NATO, European Commission, and other international funding bodies. His entrepreneurial achievements include first place in the Queen Rania National Entrepreneurship Competition (QRNEC) and leadership in technology-driven startups. His expertise in bridging innovation, academia, and enterprise continues to drive impactful research and development initiatives.



PRABAGARANE NAGARADJANE received the M.Tech. and Ph.D. degrees in ECE from Pondicherry Engineering College, Pondicherry (Central) University. He is currently an Associate Professor with the Department of Electronics and Communication Engineering, SSN Institutions. Before this, he was with HCL Info Systems for a brief period of two years. His research interests include various aspects of wireless communications, especially concerning signal

processing for wireless and broadband communications and the application of machine learning and artificial intelligence for wireless communications. He has authored or co-authored over more than 75 technical articles and two books. Recently, he visited the "Beyond 5G Wireless Innovation Center," King Mongkut's University of Technology, North Bangkok, as a Short-Term Visitor. Furthermore, he has also co-authored a research book titled *Distributed Artificial Intelligence for 5G/6G Communications*, which



currently in the press by Taylor and Francis publisher and a textbook on electronic communications for AICTE e-KUMBH. He is one of the founding members of the Wireless Communications, Signal Processing and Networking (WiSPNET) International Conference technically co-sponsored by IEEE. He also served as one of the organizing chairs of 2016, 2017, 2018, 2020, 2021, and 2022 WiSPNET and the Co-Chair of the WiSPNET 2019 Conference. Currently, he is serving as the Organizing Chair for the IEEE technically co-sponsored AsianComNet 2024 Conference to be held in Thailand. He has guest-edited two special issues on the topic of signal processing for 5G in the Computers and Electrical Engineering journal (Elsevier). He also served on the editorial board for the Physical Communication journal as an Area Editor and is currently an Associate Editor of the IET Communications journal.



**CHRISTOPHOROS CHRISTOPHOROU** received the B.Sc. degree in computer science, the M.Sc. degree in advanced computer technologies, and the Ph.D. degree in mobile/wireless networks from the University of Cyprus, in 2002, 2005, and 2011, respectively. His main research interests and expertise include the telecommunications and networking research fields but also include database management systems, social collaborative care networks, and information and communication

technology (ICT) personalized solutions (for various sectors including the eHealth domain). He has published over 35 articles in journals, scientific conferences, and book chapters. Since 2004, he has been involved initially as a Researcher and later as a Project Manager in different local (RPF-funded) and EU-funded research projects in the domain of AAL and Ageing Well, such as FRAIL, SUCCESS, MEMENTO, GrowMeUp, Miraculous-Life, SocialRobot, Co-Living, and AgeingWell; and in the mobile and wireless networks domain, such as C-CAST, C-MOBILE, MOTIVE, and BBONE.



VASOS VASSILIOU (Senior Member, IEEE) is currently an Associate Professor with the Computer Science Department, University of Cyprus (UCY), where he is also the Director of the Networks Research Laboratory (NetRL). He has been the Group Leader, since November 2017, with the Smart Networked Systems Research Group, CYENS Center of Excellence, Nicosia, Cyprus. His research interests include protocol design and performance aspects of networks (fixed, mobile,

and wireless), in particular mobility management, QoS adaptation and control, resource allocation techniques, wireless sensor networks, and the Internet of Things. He is a Senior Member of ACM. He is also in the editorial boards of the *Journal of Telecommunication Systems* (Springer) and the *Computer Networks* journal (Elsevier).



**ORESTIS NEOKLEOUS** received the M.Sc. degree in innovation design engineering from Imperial College London, the M.A. degree in innovation design engineering from the Royal College of Art, and the M.Eng. degree in electronic engineering with communications from the University of Warwick. He is currently an Interdisciplinary Innovator, an Embedded Software Engineer, and an Entrepreneur based in London, and also working with the University of Cyprus

and CYENS as an Intern. He co-founded Blurry Works, an innovation design studio, and Epicue, a venture addressing heat stress in workplaces. He is also an Embedded Software Engineer with Dotplot, developing early detection systems for breast cancer. With a strong background in machine learning, embedded systems, and software development, he has also contributed to academia as a Graduate Teaching Assistant with the Imperial College London.



ANDREAS PITSILLIDES is currently a Professor with the Department of Computer Science, University of Cyprus, the Co-Director of the Networks Research Laboratory (NetRL, http://www.NetRL.cs.ucy.ac.cy), and a Visiting Professor with the Department of Electrical and Electronic Engineering Science, University of Johannesburg, South Africa (2021–2024). He was appointed as a Visiting Professor with the School of Electrical and Information Engineering, Uni-

versity of the Witwatersrand (Wits) (2017-2020), and the Department of Electrical and Electronic Engineering Science, University of Johannesburg (2014–2017). His broad research interests include communication networks, software defined metamaterials (hypersurfaces and reconfigurable intelligent surfaces), nanonetworks and the Internet of Things and Web of Things, smart systems (e.g., smart grid), smart spaces (e.g., home, city), e-health, and adapting tools from various fields of applied mathematics, such as adaptive non-linear control theory, computational intelligence, game theory, and complex systems and nature-inspired techniques, to solve problems in communication networks. He has published over 350 refereed papers in flagship journals (e.g., IEEE, Elsevier, IFAC, and Springer), international conferences, and book chapters, co-authored two books (one edited), participated as a principal or co-principal investigator in over 40 European commission and locally funded research projects with over 6.7 million Euro, received several awards, including best paper, presented keynotes, invited lectures at major research organizations, short courses at international conferences, and short courses to industry.

. . .